Inorganic Chemistry

pubs.acs.org/IC Article

Triphenylphosphine-Modified Iridium^{III}, Rhodium^{III}, and Ruthenium^{II} Complexes to Achieve Enhanced Anticancer Selectivity by Targeting Mitochondria

Zhe Liu,* Hanxiu Fu, Heqian Dong, Kangning Lai, Zhihao Yang, Chunyan Fan, Yuting Luo, Wenting Qin, and Lihua Guo*

Cite This: *Inorg. Chem.* 2024, 63, 24736−24753 Read Online

ACCESS | Metrics & More | Article Recommendations | Supporting Information

ABSTRACT: The incorporation of an organelle-targeting moiety into compounds has proven to be an effective strategy in the development of targeted anticancer drugs. We herein report the synthesis, characterization, and biological evaluation of novel triphenylphosphine-modified half-sandwich iridium^{III}, rhodium^{III}, and ruthenium^{II} complexes. The primary goal was to enhance anticancer selectivity through mitochondrial targeting. All these triphenylphosphine-modified complexes exhibited promising cytotoxicity in the micromolar range (5.13−23.22) against A549 and HeLa cancer cell lines, surpassing the activity of comparative complexes that lack the triphenylphosphine moiety. Noteworthy is their good selectivity toward cancer cells compared to normal BEAS-2B cells, underscored by selectivity index ranging from 7.3 to >19.5. Mechanistically, these complexes primarily target mitochondria rather than interacting with DNA. The targeting of mitochondria and triggering mitochondrial dysfunction were confirmed using both confocal microscopy and flow cytometry. Their ability to depolarize mitochondrial membrane potential (MMP) and enhance reactive oxygen species (ROS) was observed, thereby leading to intrinsic apoptotic pathways. Moreover, these complexes lead to cell cycle arrest in the G_2/M phase and demonstrated antimigration effects, significantly inhibiting the migration of A549 cells in wound-healing assays.

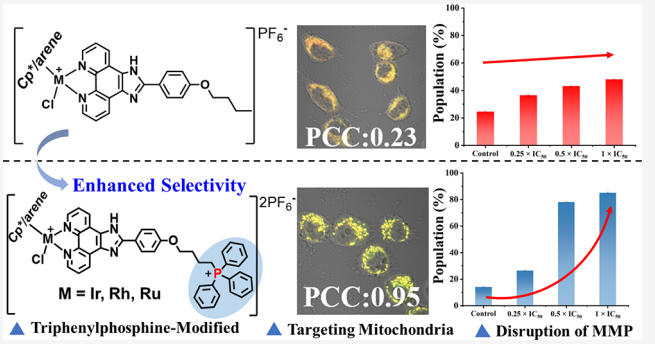

Downloaded via MOSCOW STATE UNIV on May 12, 2026 at 11:28:25 (UTC).
See https://pubs.acs.org/sharingguidelines for options on how to legitimately share published articles.

1. INTRODUCTION

Cancer remains a leading cause of mortality and a significant barrier to an increasing global life expectancy. Despite various available treatments, chemotherapy continues to be a crucial and indispensable option for cancer management. Platinum-based medications, including cisplatin, carboplatin, and oxaliplatin, are well-known for their efficacy in treating diverse tumors.[1,2] However, these anticancer agents often suffer from a lack of selectivity, significant adverse effects, and the potential for developing resistance.[3−5] Consequently, identifying new targets for anticancer drug action and developing novel anticancer agents remain central research priorities in cancer therapy.[6−8] Organelle-targeted antitumor drugs can effectively address these problems and have become one of the hotspots in current antitumor drug research.[9−16] Notably, considering that numerous conditions, including cancer, diabetes, neurodegenerative diseases, and ischemia−reperfusion injury, are linked to mitochondrial dysfunction, there has been an increasing focus on targeting mitochondria in drug development over the past two decades.[17−19]

Mitochondria are crucial organelles that are primarily responsible for energy production within cells. Additionally, they play roles in various other cellular processes, including generating reactive oxygen species (ROS), disrupting mitochondrial membrane potential (MMP), storing calcium ions, and facilitating apoptosis mediated by mitochondrial pathways.[20,21] Mitochondrial targeting represents a strategic focus on organelle-specific intervention.[22] Triphenylphosphine is a commonly used mitochondria-targeting lipophilic cation, composed of a positively charged phosphonium ion and three phenyl rings that enhance its lipophilicity.[23] The phenyl rings are spatially positioned to shield the phosphorus atom from dissolution. Additionally, the positive charge on the phosphorus atom is distributed across the three phenyl rings, creating a delocalized positive charge that facilitates the passage of triphenylphosphine through the lipid bilayer, allowing it to specifically target the interior of mitochondria.[24−26] The first organic small molecule of its kind, methyl-

Received: September 19, 2024
Revised: November 13, 2024
Accepted: December 2, 2024
Published: December 16, 2024

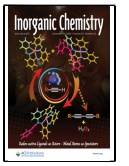

ACS Publications © 2024 American Chemical Society

https://doi.org/10.1021/acs.inorgchem.4c03975
Inorg. Chem. 2024, 63, 24736−24753

Scheme 1. Known Triphenylphosphine-containing Compounds, Half-Sandwich Complexes, and Our Current Work

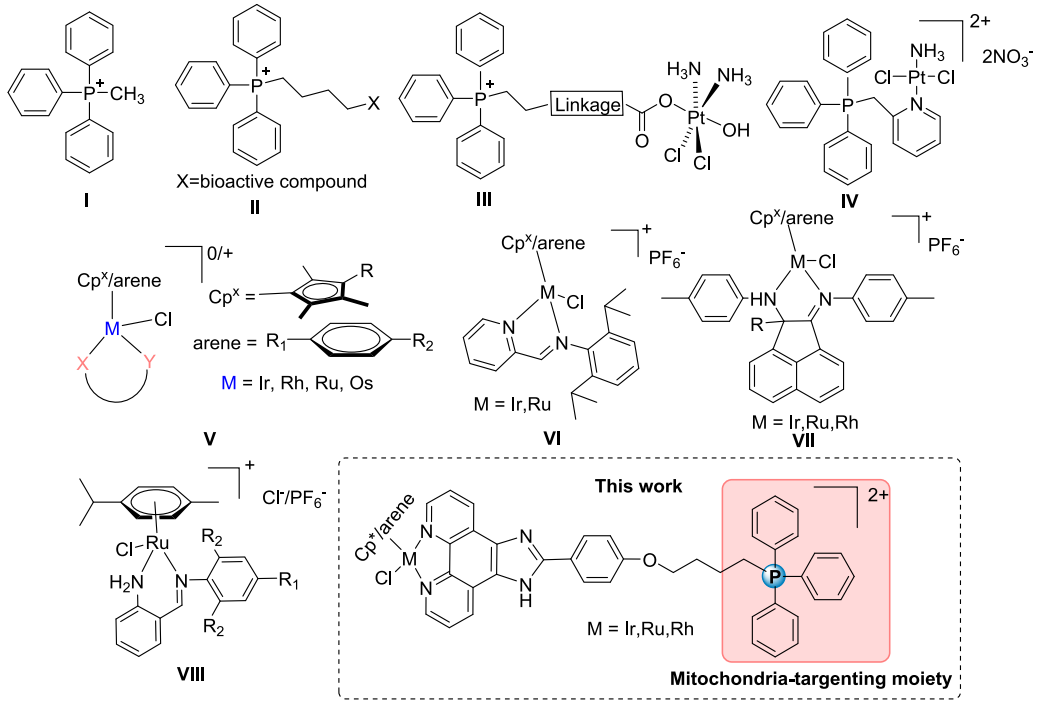

triphenylphosphonium (TPP) cation, selectively accumulates in mammalian cell mitochondria in response to higher membrane potentials (Scheme 1, I).[27,28] The delivery of drugs to mitochondria was optimized by directly attaching bioactive molecules to TPP using alkyl chains or other covalent bonds, refining their application in mitochondrial biology (Scheme 1, II).[29−31]

In particular, TPP and its derivatives have also been employed, although remain scarce, as building blocks or chelating ligands to develop metal-based agents for anticancer or antimicrobial applications.[31−34] For example, when cisplatin is conjugated with TPP (Scheme 1, III and IV), it preferentially targets mitochondria rather than nuclear DNA, integrating into the mitochondrial genome to influence cellular functions.[33,34] This strategy also effectively overcame cisplatin resistance.[33] Generally, the mitochondrion-targeting system, driven by triphenylphosphine and leveraging mitochondrial membrane potential, is designed to direct drugs preferentially to the mitochondria of cancer cells. The hyperpolarization of both the cancer cell membrane and mitochondrial membranes enables selective drug accumulation at these sites. This strategy not only increases the direct cytotoxic effects on cancer cells but also minimizes potential toxicity to normal cells.[35]

In recent years, half-sandwich organometallic complexes, particularly those based on iridium^{III}, rhodium^{III}, ruthenium^{II} and osmium^{II} with the structural type $[(\eta^6\text{-arene})/(\eta^5\text{-Cp*})M(XY)Cl]^{0/+}$ (where Cp* represents $C_5(CH_3)_5$ and XY denotes bidentate chelating ligands), have garnered significant interest in cancer research (Scheme 1, V).[36−39]

These complexes are celebrated for their modifiable structure, which allows for a rich diversity of molecular structures and biological activities. Unlike traditional platinum-based drugs, these metal complexes follow distinct mechanisms of action, potentially overcoming platinum resistance and reducing toxicity. Notably, the ruthenium^{II} complexes NAMI-A and KP1019 have demonstrated promising outcomes in both preclinical and clinical trials, positioning them as potential drug candidates.[40,41] However, most of these complexes continue to suffer from unclear targets and mechanisms of actions (MoAs), coupled with limited selectivity between normal and cancerous cells.[42,43] Our group is committed to advancing the development of organometallic complexes of iridium^{III}, rhodium^{III}, and ruthenium^{II} with N^N chelating ligands.[44−48] Notably, some of the imine−pyridyl (Scheme 1, VI) and imine−amine (Scheme 1, VII and VIII) complexes have shown promising cytotoxic effects and displayed anticancer selectivity against A549 cancer cells relative to BEAS-2B normal cells, mediated by a ROS-based redox mechanism.[48−50] These encouraging results have inspired us to explore new platinum group metal-based anticancer complexes through the coupling with the triphenylphosphonium (PPh^{3+}) moiety, potentially combining the advantages of mitochondria-targeting ability of PPh^{3+}moiety and specific properties of half-sandwich metal complexes (Scheme 1). Herein, we synthesized a series of triphenylphosphine-modified half-sandwich iridium^{III}, rhodium^{III}, and ruthenium^{II} complexes, specifically designed to target mitochondria. This targeting ability appears to enhance the generation of reactive oxygen species (ROS), disrupt mitochondrial membrane potential (MMP), and trigger apoptosis in cancer cells, leading to selective cytotoxic effects on A549 cancer cells compared with normal BEAS-2B cells.

2. RESULTS AND DISCUSSION

2.1. Synthesis and Characterizations. The chloro-bridged bimetallic iridium^{III} precursor **D1** ($[(\eta^5\text{-Cp*})IrCl_2]_2$), rhodium^{III} precursor **D2** ($[(\eta^5\text{-Cp*})RhCl_2]_2$), and ruthenium^{II} precursor **D3** ($[(\eta^6\text{-}p\text{-cymene})RuCl_2]_2$) were synthesized following established methods in the literature.[51−53] The phenanthroline-based N^N chelating ligand **L1** was synthesized in a moderate yield by the reaction of (4-(4-formylphenoxy)-butyl) triphenylphosphonium bromide with 1,10-phenanthroline-5,6-dione and the excess ammonium acetate using a

https://doi.org/10.1021/acs.inorgchem.4c03975
Inorg. Chem. 2024, 63, 24736−24753

Scheme 2. Synthesis of Ligands L1 (a), Synthesis of Half-Sandwich Iridium^{III}, Rhodium^{III}, and Ruthenium^{II} Complexes (b), and the Detailed Structures of Ir1, Ir2, Rh1, Rh2, Ru1, and Ru2 (c)

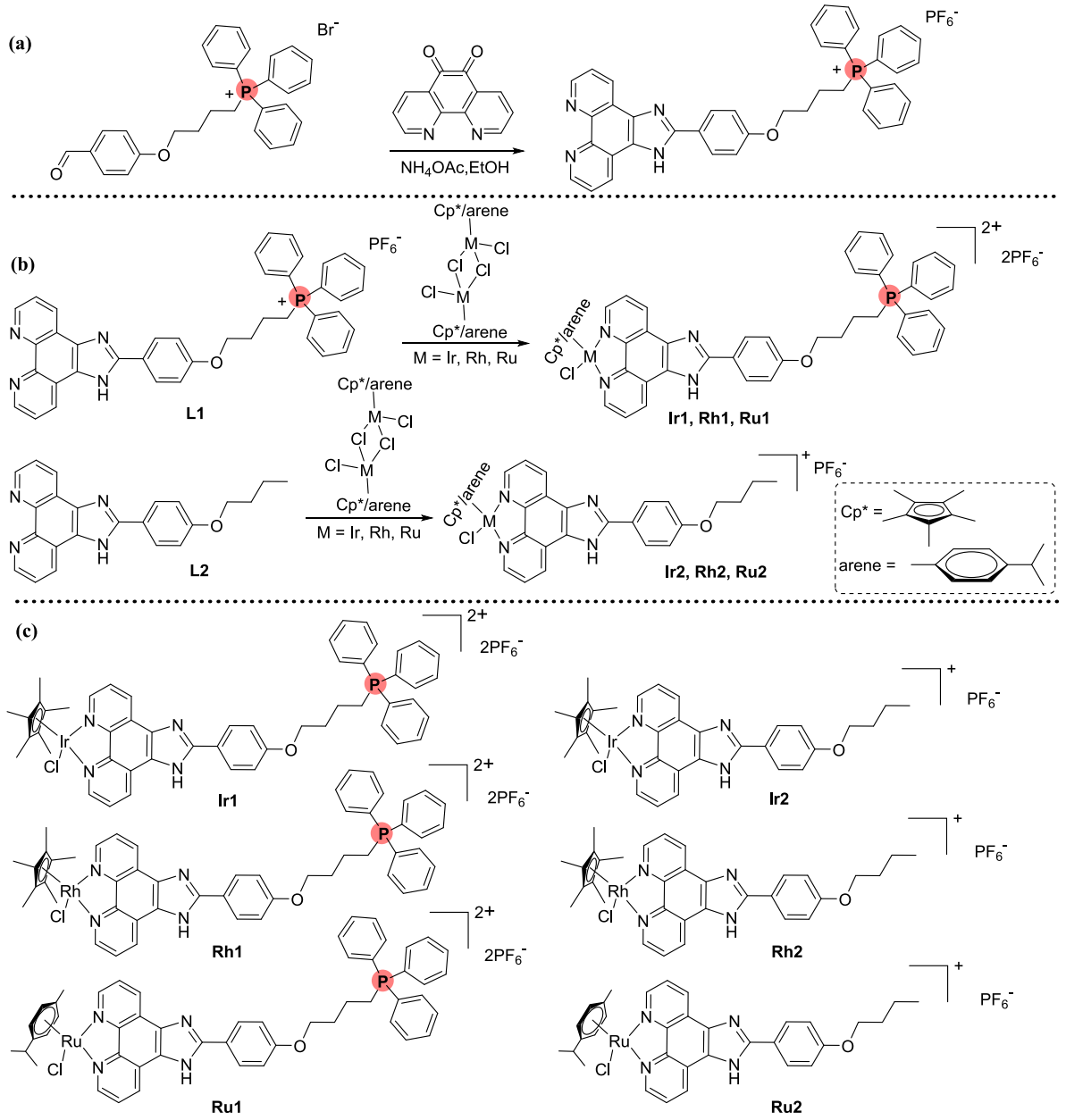

modified procedure (Scheme 2a). **L2**, which did not contain triphenylphosphine moiety, was also prepared following literature method.[32] The triphenylphosphine-modified complexes **Ir1**, **Rh1**, and **Ru1** were synthesized in 59−71% yields by reacting the metal precursors **D1**, **D2**, or **D3** with the corresponding ligands in a solution of CH_2Cl_2 and CH_3OH (v/v = 1:1) (Scheme 2b). For comparison, complexes **Ir2**, **Rh2**, and **Ru2**, which lack the triphenylphosphine moiety, were similarly prepared (Scheme 2b). The formation of these complexes were fully confirmed by ^1H, ^{13}C, and ^{31}P NMR (Figures S4−S21), elemental analysis and mass spectroscopy (positive mode: Figures S22−S27 and negative mode: Figures S28−S30). In the ^1H NMR spectra of these complexes, molar equivalents of bound Cp*/arene per mole of ligand were detected, indicating coordination between the ligands and the metal ions. ^{31}P NMR analysis distinctly shows that in the complexes **Ir1**, **Rh1**, and **Ru1** the triphenylphosphine (PPh^{3+}) moiety and the PF_6^- counteranion produce a singlet and a septet at approximately δ20 and −140 ppm, respectively (Figure 1). Conversely, only a septet, corresponding to the PF_6^- counteranion, was observed in complexes **Ir2**, **Rh2**, and **Ru2** without triphenylphosphine moiety (Figures S9, S14, and S21). This result further validates the successful synthesis of the targeted complexes. Particularly, the variation of the metal center (**Ir1** vs **Rh1** vs **Ru1**) has minimal impact on the chemical shifts in the ^{31}P NMR spectra. Unfortunately, despite numerous attempts, we have been unable to successfully crystallize these metal complexes into single crystals.

2.2. Absorption and Emission Spectroscopy. UV−visible (UV−vis) absorption spectra for these iridium^{III}, rhodium^{III}, and ruthenium^{II} complexes were recorded in methanol at 37 °C (Figure 2a). A prominent absorption peak was noted between 270 and 298 nm across these complexes. Further, broader and less intense absorption peaks

https://doi.org/10.1021/acs.inorgchem.4c03975
Inorg. Chem. 2024, 63, 24736−24753

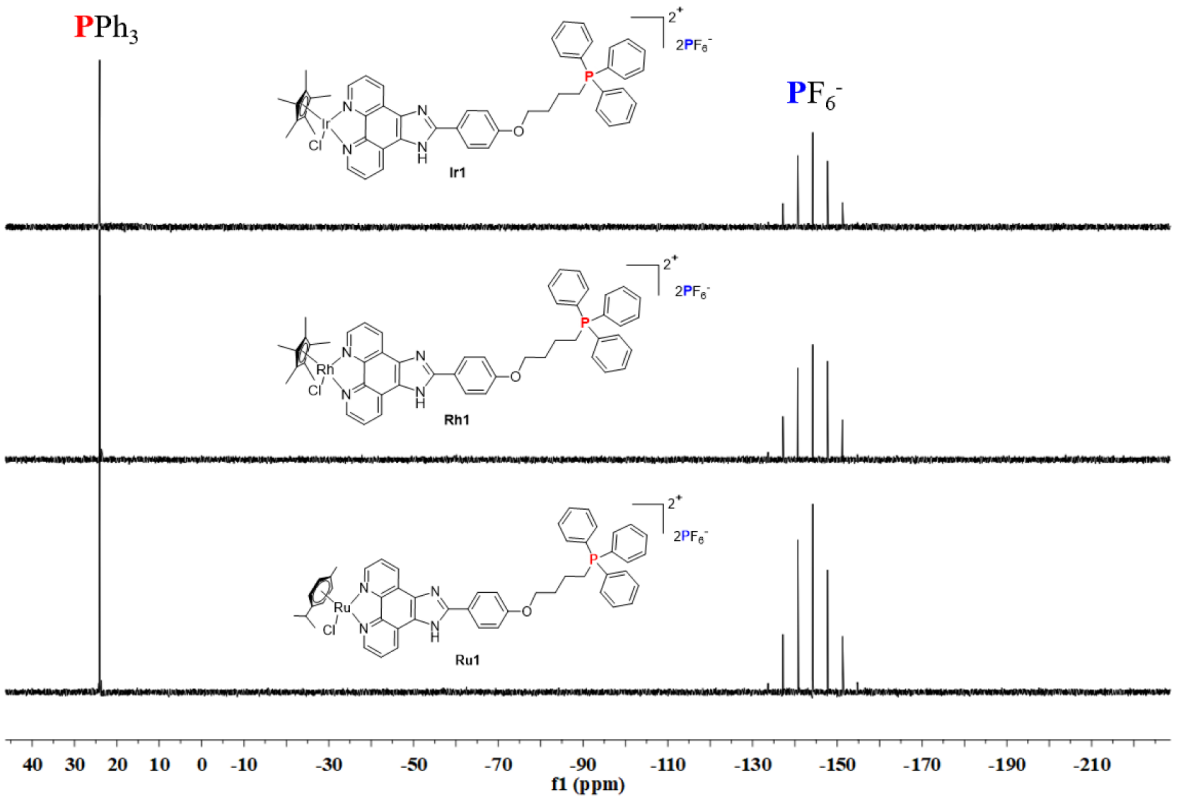

Figure 1. ^{31}P NMR spectrum of phosphorus complexes **Ir1**, **Rh1**, and **Ru1**.

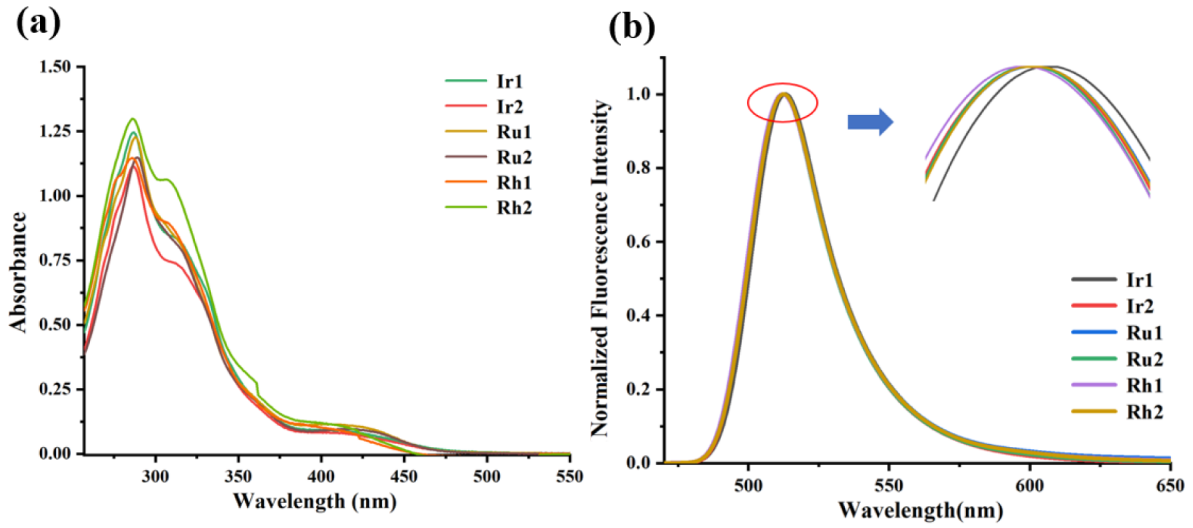

Figure 2. (a) UV−visible absorbance spectra of **Ir1**, **Ir2**, **Rh1**, **Rh2**, **Ru1**, and **Ru2** (20 μM) in MeOH solutions at 37 °C. (b) Normalized emission spectra of **Ir1**, **Ir2**, **Rh1**, **Rh2**, **Ru1**, and **Ru2** (20 μM) in MeOH at 37 °C.

around approximately 310 and 410 nm were also detected. The peaks observed below 300 nm are indicative of ligand-centered $\pi-\pi^*$ transitions, while those between 300 and 450 nm are typically associated with metal-to-ligand charge transfer or $d-d$ transitions, which is consistent with those reported in other half-sandwich iridium^{III}, rhodium^{III}, and ruthenium^{II} complexes.[54−56] The absorption spectra for these complexes show comparable features, indicating that changes in the metal ion and ligand substitution have little effect on their spectral absorption bands.

When excited at λ_{ex} = 286−290 nm, the complexes **Ir1**, **Ir2**, **Rh1**, **Rh2**, **Ru1**, and **Ru2** exhibited emission peaks (λ_{em}) between 511 and 513 nm (**Ir1**: 512 nm, **Ir2**: 513 nm, **Rh1**: 512 nm, **Rh2**: 511 nm, **Ru1**: 512 nm, and **Ru2**: 513 nm) at 37 °C in methanol (Figure 2b). Consistent emission patterns across these spectra also suggest a minimal influence of the metal center and ligand variations on the emission bands. The emission quantum yields of **Ir1**, **Rh1**, and **Ru1** are notably low in methanol solutions (**Ir1**: 0.12%, **Rh1**: 0.27%, and **Ru1**: 0.24%), with fluorescein used as the reference standard. Additionally, the average lifetimes of **Ir1**, **Rh1**, and **Ru1** were recorded at 5.14, 5.50, and 4.75 ns respectively (Figure S31), indicating their fluorescent properties. Notably, this weak photoluminescence is consistent with observations in other

https://doi.org/10.1021/acs.inorgchem.4c03975
Inorg. Chem. 2024, 63, 24736−24753

reported half-sandwich iridium^{III}, rhodium^{III}, and ruthenium^{II} complexes.[46,56,57] However, the photoluminescent characteristics of these complexes provide a potential method for observing their cellular localization and accumulation, which could offer detailed insights into their MoAs.

2.3. Solution Stability. To evaluate the stability of **Ir1**, **Ir2**, **Rh1**, **Rh2**, **Ru1**, and **Ru2** in aqueous solutions, hydrolysis experiments were conducted in a solution of 80% DMSO-d_6/20% PBS (pH ≈ 7.4, made with D_2O) (v/v) at 37 °C, using ^{1}H NMR analysis. Given their limited solubility at high water content, a higher proportion of DMSO-d_6 was used to maintain a sufficient complex concentration for reliable spectroscopic measurement. Over a 24 h period, no additional peaks were detected in the ^{1}H NMR spectra, and the proton assignments remained consistent with their established molecular structures (Figures S32−37). This indicates that the complexes did not undergo decomposition or ligand dissociation, demonstrating their stability under the tested low-water content conditions.

The stability of the complexes **Ir1**, **Ir2**, **Rh1**, **Rh2**, **Ru1**, and **Ru2** was also evaluated at 37 °C in a solution of 10% DMSO/90% PBS (v/v, pH ≈ 7.4, prepared with H_2O, high water content solution) using UV−vis spectroscopy across various time intervals over a 24-h period. While no significant shifts in the absorption bands were noted, there were changes in the absorption intensity of these complexes (Figure S38). This behavior suggests hydrolysis of the metal-Cl bond (Cl^-/H_2O exchange), aligning with observations from other reported half-sandwich iridium^{III}, rhodium^{III}, and ruthenium^{II} complexes that feature monodentate labile chloride ligands.[48,58] This outcome through UV−vis analysis appears to be inconsistent with the NMR results. However, in line with the trends noted in earlier studies of half-sandwich metal complexes,[59,60] these complexes are likely to undergo Cl^-/H_2O exchange more readily in diluted solutions with high water content, akin to typical cell culture conditions. Significantly, the hydrolysis of the metal−Cl bond often acts as an activation step for many anticancer complexes.[59] The half-lives ($t_{1/2}$) and hydrolysis rate constants (k) were calculated for these complexes by fitting the changes in absorption to pseudo-first-order kinetics (Table 1). Overall,

Table 1. The Half-Life and Hydrolysis Rate of Iridium^{III}, Rhodium^{III}, and Ruthenium^{II} in Different Solvent Systems

	10% DMSO/90% PBS pH ≈ 7.4		10% DMSO/90% PBS pH ≈ 5.5	
Complexes	$t_{1/2}$ (min)	k (min^{-1})	$t_{1/2}$ (min)	k (min^{-1})
Ir1	120.75	0.00574	149.06	0.00462
Ir2	116.10	0.00597	139.19	0.00498
Rh1	200.33	0.00346	276.15	0.00251
Rh2	133.55	0.00519	152.01	0.00456
Ru1	155.41	0.00446	141.17	0.00491
Ru2	117.08	0.00592	121.81	0.00569

these complexes underwent relatively slow hydrolysis, with half-lives ranging from 116.1 to 200.3 min, demonstrating a slower rate of hydrolysis compared to some reported half-sandwich iridium^{III}, rhodium^{III}, and ruthenium^{II} complexes with N,N-donor ligands.[48,61] The hydrolysis rates for these complexes follow a decreasing order: **Ir2** > **Ir1**, **Rh2** > **Rh1**, and **Ru2** > **Ru1**, indicating that the introduction of the triphenylphosphine moiety into these complexes effectively reduces chloride loss. Additionally, to assess the stability of the complexes in the acidic environment characteristic of cancer cells, we prepared a buffered solution using 10% DMSO/90% PBS (v/v), adjusting the pH to approximately 5.5 with an acetic acid/sodium acetate buffer, and conducted stability tests. The results showed that this pH adjustment did not significantly impact the hydrolysis rate of the complexes (Figure S39, Table 1). Overall, the potential stability of these complexes for further investigation of their anticancer activity under aqueous conditions has been confirmed.

2.4. Cytotoxicity. Using cisplatin as a reference, the cytotoxicity of complexes **Ir1**, **Ir2**, **Rh1**, **Rh2**, **Ru1**, and **Ru2** toward A549 lung cancer cells, cervical carcinoma HeLa cells, and noncancerous BEAS-2B cells was assessed via MTT assay (Table 2). The precursors **D1**−**D3** and ligands **L1**−**L2** showed

Table 2. IC_{50} Values of Ligands, Precursors, and Complexes Tested Toward Cancer and Normal Cell Lines and Their Comparison with Cisplatin

	IC_{50} (μM)			
Complexes	A549	HeLa	BEAS-2B	SI[a]
L1	>100	>100	>100	-
L2	>100	>100	>100	-
D1	>100	>100	>100	-
D2	>100	>100	>100	-
D3	>100	>100	>100	-
Ir1	5.13 ± 0.25	12.78 ± 0.12	>100	>19.5
Ir2	46.28 ± 0.24	28.34 ± 0.18	51.21 ± 0.14	1.1
Ru1	6.25 ± 0.18	12.79 ± 0.20	82.34 ± 0.22	13.2
Ru2	43.72 ± 0.19	31.89 ± 0.13	46.28 ± 0.11	1.1
Rh1	12.50 ± 0.23	23.22 ± 0.17	91.41 ± 0.09	7.3
Rh2	33.85 ± 0.17	32.29 ± 0.06	46.28 ± 0.24	1.4
Cisplatin	24.89 ± 0.21	8.39 ± 0.08	29.21 ± 0.22	1.2

[a]SI: The selectivity index represents the IC_{50} ratio of BEAS-2B normal cells to A549 cancer cells. Data are quoted as mean ± standard deviation (SD) of three replicates. Statistical analysis using t test indicated a significant difference in IC_{50} values between A549 and BEAS-2B cells for **Ir1**, **Ir2**, **Ru1**, **Ru2**, **Rh1** and **Rh2** (*p < 0.05).

no obvious cytotoxicity toward A549 and HeLa cancer cells (IC_{50} > 100 μM). In contrast, all tested complexes exhibited effective cytotoxicity toward A549 and HeLa cancer cells, with IC_{50} values in a range of 5.13−46.28 μM, surpassing or matching the efficacy of cisplatin. Thus, this anticancer effectiveness is ascribed to the chelation between the free ligands and the iridium^{III}, rhodium^{III}, and ruthenium^{II} ion. **Ir1**, **Rh1**, and **Ru1** featuring the triphenylphosphine moiety, exhibited significantly enhanced potency (3 to 9 times greater) against A549 cells compared to their counterparts **Ir2**, **Rh2**, and **Ru2** with IC_{50} values of 5.13−12.50 μM versus 33.85−46.28 μM. A similar trend was also observed in Hela cells, where, although the increase in cytotoxicity was less pronounced than in A549 cells, the potency still reached 1.5 to 3 times higher (12.78−23.22 μM versus 28.34−32.29 μM). Basically, under the same ligand conditions, variations in the metal center had minimal impact on the cytotoxicity exhibited by these complexes toward the same cancer cell lines, suggesting that the ligand environment predominantly dictates their anticancer activity. A distinctive feature of these triphenylphosphine-modified complexes is their enhanced selectivity between cancerous and normal cells. **Ir1** was inactive (IC_{50} > 100 μM) toward noncancerous BEAS-2B cells and showed a selectivity index (SI) of >19.5 toward A549

https://doi.org/10.1021/acs.inorgchem.4c03975
Inorg. Chem. 2024, 63, 24736−24753

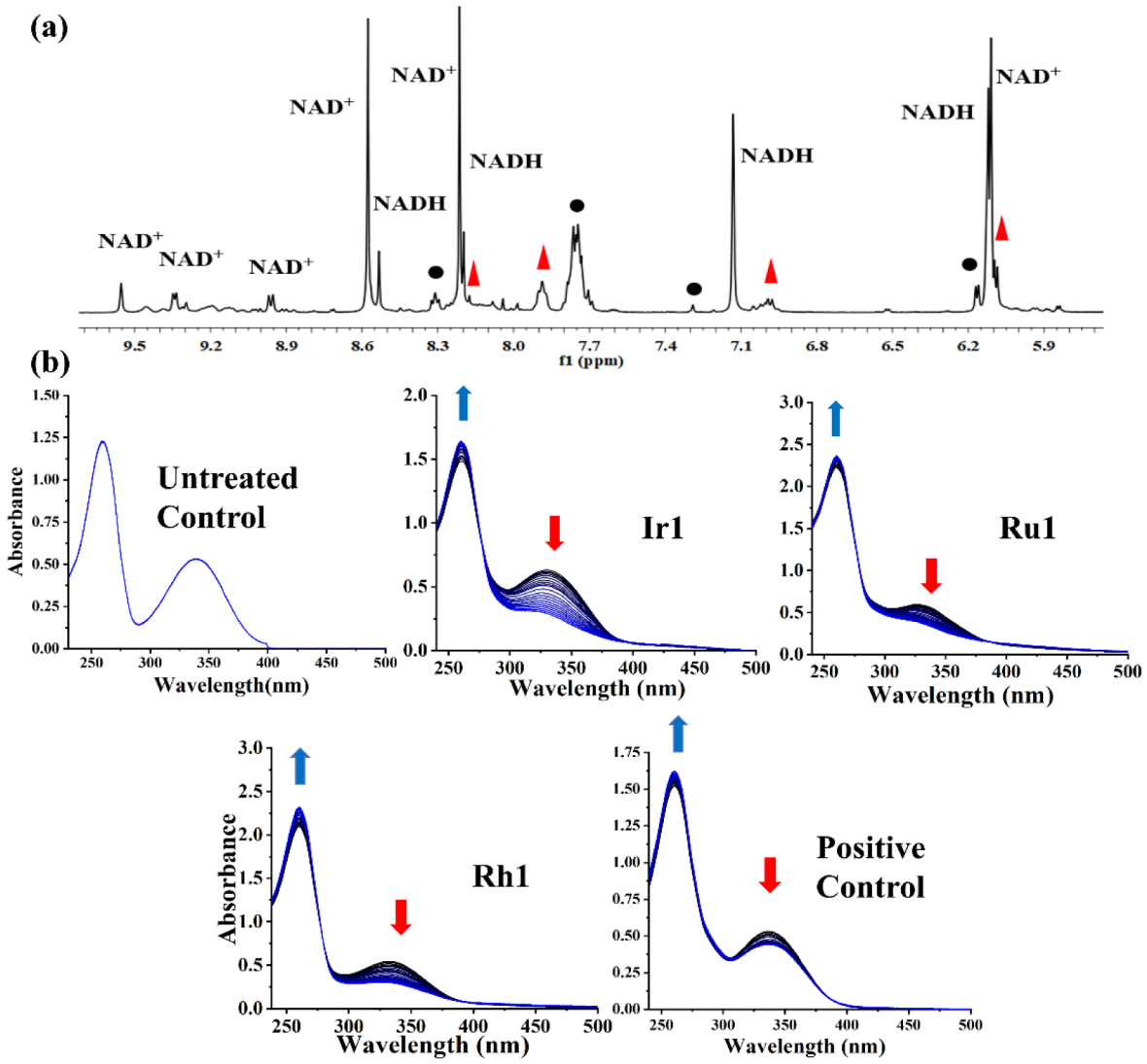

Figure 3. (a) ^{1}H NMR spectrum of complex **Ir1** (1 mM) and NADH (5 mM) in CD_3OD and D_2O (v/v 4:1) at 37 °C after 15 min. Peaks labeled (red solid triangle) and (black solid circle) correspond to the formed Ir−H complex and chlorido complex **Ir1**. (b) UV−vis spectra of the reaction of NADH (100 μM) with **Ir1**, **Rh1**, and **Ru1** and positive control (Cp*Ir(phpy)Cl) (1 μM) in 10% MeOH/90% H_2O (v/v) at 25 °C for 8 h.

and BEAS-2B cells. Moreover, complexes **Rh1** and **Ru1** exhibited minimal cytotoxicity toward BEAS-2B cells, with IC_{50} values that were 7.3 and 13.2 times higher, respectively, than those observed in A549 cancer cells. Conversely, the complexes **Ir2**, **Rh2**, and **Ru2** without a triphenylphosphine moiety showed no significant selectivity between cancer and normal cells. Thus, it seemed that the introduction of the triphenylphosphine moiety in this system led to both the enhanced cytotoxicity and improved selectivity of these complexes.

The highly lipophilic nature of triphenylphosphine led us to explore whether the cytotoxicity of these complexes is influenced by their lipophilicity. Consequently, the octanol/water partition coefficients (log P) for these complexes were measured by using the shake-flask method. The resulting log P values displayed the following trend: **Ir1** (1.55) > **Ir2** (0.75), **Rh1** (0.97) > **Rh2** (0.61), and **Ru1** (1.28) > **Ru2** (0.68). In cancer cells, a consistent trend was observed, indicating that the cytotoxicity of these complexes correlated to their lipophilicity was observed. However, in normal BEAS-2B cells, the cytotoxicity of **Ir2**, **Rh2**, and **Ru2** was approximately twice as high as that of **Ir1**, **Rh1**, and **Ru1**, indicating that lipophilicity may not be the only factor influencing their cytotoxicity and selectivity. This discrepancy points to the potential role of redox-based mechanisms, as supported by our observations in subsequent biological experiments (catalytic oxidation of NADH to NAD^+, mitochondria targeting, mitochondrial dysfunction, and ROS generation).

2.5. DNA and Protein Binding Results. Given that the cytotoxic effects of many anticancer complexes are related to DNA binding, the capability of complexes **Ir1**, **Rh1**, and **Ru1** to bind with the model nucleobase 9-methyladenine (9-MeA) was initially assessed using ^{1}H NMR spectroscopy in a solution of 80% DMSO-d_6/20% D_2O. Over 24 h, no interactions were detected between the complexes and 9-MeA under the experimental conditions (Figures S40−S42). Additionally, mass spectrometry analysis confirmed the absence of any nucleobase adducts. The interactions of complexes **Ir1**, **Rh1**, and **Ru1** with CT-DNA were subsequently examined by using UV−vis absorption spectroscopy (Figure S43). The experiments involved adding increasing concentrations of CT-DNA (0−43.6 μM) to solutions containing 60 μM of each complex.

https://doi.org/10.1021/acs.inorgchem.4c03975
Inorg. Chem. 2024, 63, 24736−24753

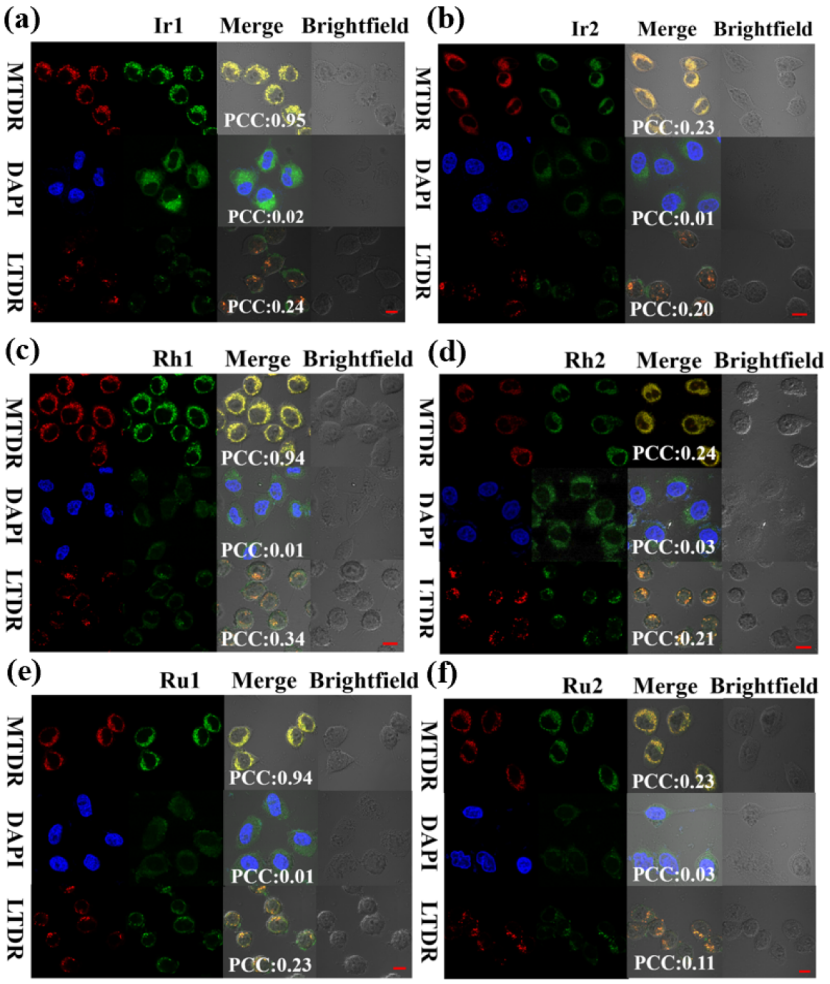

Figure 4. Determination of intercellular localization of **Ir1** (a), **Ir2** (b), **Rh1** (c), **Rh2** (d), **Ru1** (e), **Ru2** (f) by confocal microscopy. A549 cells were incubated with **Ir1**, **Rh1**, and **Ru1** (2 μM) for 1 h at 37 °C, then coincubated with DAPI (1 μg/mL), MTDR (500 nM) or LTDR (75 nM) for 1 h, respectively. Scale bar: 20 μm. The green, red, and blue fluorescence represent **Ir1**, **Rh1**, and **Ru1**, mitochondria, lysosome, and nucleus, respectively.

This increase in CT-DNA concentration resulted in hyperchromism and a slight red shift at the absorption peak, typically indicative of noncovalent electrostatic binding.[62,63] Additionally, the Benesi−Hildebrand equation was applied to determine the intrinsic equilibrium binding constants (K_b) of these complexes with CT-DNA. The determined K_b values ranged from 5.88×10^3 to 1.60×10^4 M^{-1} (**Ir1**: $K_b = 1.02 \times 10^4$, **Rh1**: $K_b = 1.60 \times 10^4$ M^{-1}, **Ru1**: $K_b = 5.88 \times 10^3$ M^{-1}). These values were notably lower than those of previously reported half-sandwich complexes ($K_b > 10^5$ M^{-1}),[64−66] suggesting a relatively weak interaction with CT-DNA. Furthermore, the binding affinity values (K_b) of **Ir1**, **Rh1**, and **Ru1** also did not correlate with their cytotoxicity toward cancer cells, indicating that DNA binding might not be the predominant mechanism of action for these half-sandwich complexes. This speculation is further reinforced by the observed low colocalization efficiency of these complexes within the nucleus (see Section 2.7 below).

Bovine serum albumin (BSA) serves as an economical model for investigating the interactions between anticancer agents and blood plasma proteins due to its plentiful presence in plasma, exceptional binding properties, and similarity to human serum albumin (HSA).[67] BSA is known to bind a wide range of substrates, including hormones, metal cations, and many therapeutic drugs.[68] Consequently, exploring the reactions of anticancer metallodrugs with proteins is essential for understanding their toxicity, biodistribution, and mechanisms of action within this novel class of anticancer agents. The binding affinity of complexes **Ir1**, **Rh1**, and **Ru1** with BSA was assessed using UV−vis absorption and fluorescence spectroscopy (Figures S44 and S46). To reduce self-absorption, both the reference and sample cuvettes were treated with the respective complexes. BSA's fluorescence is primarily derived from tyrosine (Tyr) and tryptophan (Trp), two aromatic amino acids that are sensitive to environmental changes. When small-molecule complexes interact with these residues, a reduction in the fluorescence emission is typically observed. As the concentrations of **Ir1**, **Rh1**, and **Ru1** increased, a decrease and red shift in the absorption peak at 233 nm were observed (Figure S44a−c), likely due to α-helix disruptions and the effects of polar solvents.[69] Moreover, a consistent increase with no shift was noted in BSA's absorption peak at 279 nm for these complexes, indicating subtle changes in the surrounding environment of the aromatic amino acid residues in BSA (Tyr and Trp).[70] Additionally, the fluorescence intensity of BSA consistently decreased at 353 nm as the concentration of the complexes increased (Figure S44d−f),

https://doi.org/10.1021/acs.inorgchem.4c03975
Inorg. Chem. 2024, 63, 24736−24753

suggesting that the interaction with BSA occurs through a static quenching mechanism.[71,72]

Synchronous fluorescence spectrometry proves essential for examining the conformational changes in BSA upon interaction with the complexes. Maintaining a fixed wavelength interval of either 15 or 60 nm enables the detection of specific changes in the Trp or Tyr residues of BSA. Specifically, the emission wavelength for Trp decreased at 273 nm ($\Delta\lambda$ = 60 nm) with a 5 nm red shift, while the emission for Tyr showed a decrease at 288 nm ($\Delta\lambda$ = 15 nm) with a minor red shift of 2 nm (Figure S45). These results suggest that complexes **Ir1**, **Rh1**, and **Ru1** predominantly influence the conformation of the Trp microregion when they interact with BSA.

2.6. Catalytic Hydride Transfer. Nicotinamide adenine dinucleotide (NADH) and its oxidized counterpart, NAD^+, are crucial for cellular homeostasis. The NADH/NAD^+ ratio and NAD^+ concentration are integral to various intracellular redox processes. Cancer cells typically undergo oxidative stress due to elevated levels of oxidizing species generated by their active metabolism.[73] Consequently, they are more sensitive to fluctuations in the NADH/NAD^+ ratio and NAD^+ concentrations than normal cells. Manipulating the NADH/NAD^+ balance with catalytic anticancer complexes could enhance selectivity toward cancer cells over normal cells. The use of hydride transfer catalysis in cancer drug design has been extensively explored recently.[74] In light of these considerations, we examined the interactions of **Ir1**, **Rh1**, and **Ru1** with NADH via ^{1}H NMR spectroscopy. NADH (5 equiv) was added to the solutions of **Ir1** (Figure 3a), **Rh1** (Figure S46), and **Ru1** (Figure S47), each at a concentration of 1 mM, in a mixture of CD_3OD and D_2O (4:1 v/v). This led to the appearance of new NMR peaks at 9.0, 9.3, and 9.6 ppm, corresponding to the oxidized form of NAD^+ (Figure 3a). However, after 12 h, no peaks associated with Ir−H, Rh−H, and Ru−H hydrides were observed, likely due to the instability of these hydride adducts.[75] Subsequently, we assessed the interaction of **Ir1**, **Rh1**, **Ru1**, and Cp*Ir(phpy)Cl (phpy = phenylpyridine, as a positive control)[76] with NADH at a 1:100 molar ratio in a solution of 10% MeOH/90% H_2O (v/v) using UV−vis spectroscopy (Figure 3b). Compared to the untreated control group without metal complex catalysts, the presence of **Ir1**, **Rh1**, **Ru1**, and Cp*Ir(phpy)Cl catalysts led to a noticeable decrease in the intensity of the NADH absorption band at 339 nm over an 8 h period, confirming that the observed effects were indeed attributable to catalytic action rather than external factors. The turnover numbers (TON) were calculated as 40.07 for **Ir1**, 38.90 for **Rh1**, 28.30 for **Ru1**, and 14.15 for Cp*Ir(phpy)Cl. The significantly higher TON values for **Ir1**, **Rh1**, and **Ru1** compared to those of Cp*Ir(phpy)Cl demonstrate that the catalytic efficiency of these new complexes exceeds that of Cp*Ir(phpy)Cl. Notably, previous studies have demonstrated that the catalytic oxidation of NADH to NAD^+ increases ROS levels, thereby providing an oxidative mechanism of action.[77,78] Consequently, the ability of these complexes to produce ROS in both cancer and normal cells was further explored in follow-up experiments (Section 2.9).

2.7. Cellular Localization and Cellular Uptake Pathway. Confocal microscopy was used for intracellular localization analysis to determine the potential targets of these complexes (Figure 4a−f). Probes, such as 4,6-diamino-2-phenyl indole (DAPI) for the nucleus, Mito Tracker Red CM-H2XRos (MTDR) for mitochondria, and Lyso Tracker Red DND-99 (LTDR) for lysosomes, were used.[79] A549 cells were simultaneously stained with organelle-specific probes and the corresponding complexes. Following a 1 h treatment, distinct green fluorescence was observed in the cytoplasm, indicating effective penetration of these complexes into A549 cells. All of these complexes exhibited minimal colocalization with DAPI and LTDR, evidenced by low Pearson correlation coefficient (PCC) values (PCC = 0.01−0.03 for DAPI and PCC = 0.11−0.34 for LTDR). Thus, these complexes did not localize effectively within the nucleus or lysosomes. However, the complexes **Ir1**, **Rh1**, and **Ru1**, which contain the triphenylphosphine moiety, effectively accumulate in mitochondria, as indicated by high PCC values (Figure 4a,c, and e, **Ir1**: PCC = 0.95; **Rh1**: PCC = 0.94; **Ru1**: PCC = 0.94). In contrast, **Ir2**, **Rh2**, and **Ru2**, lacking the triphenylphosphine moiety, showed a negligible degree of merging with mitochondria (Figure 4b, d and f, **Ir2**: PCC = 0.23; **Rh2**: PCC = 0.24 **Ru2**: PCC = 0.23). The comparison of colocalization coefficients reveal that incorporating triphenylphosphine significantly enhances the complexes' targeting of mitochondria, suggesting that the cytotoxicity of these complexes might be attributed to mitochondria-mediated cell death. Given that cancer cells possess more mitochondria than normal cells, they are more susceptible to mitochondrial disruption. This differential sensitivity may contribute to the anticancer selectivity of these complexes with a triphenylphosphine moiety. Notably, the complexes **Ir1**, **Rh1**, and **Ru1** demonstrated significantly higher positive zeta potentials—44.99 ± 0.19, 50.95 ± 0.22 and 20.56 ± 0.32 respectively (Figure S48), compared to the negative zeta potentials of **Ir2**, **Rh2**, and **Ru2**—−6.27 ± 0.12, −13.83 ± 0.21, and −6.61 ± 0.16 respectively (Figure S49). This characteristic could enhance their targeting of mitochondria, which possess negatively charged surfaces, upon entry into the cytosol. The higher positive zeta potentials of **Ir1**, **Rh1**, and **Ru1** may facilitate their accumulation in the mitochondria of cancer cells, which typically exhibit higher mitochondrial membrane potentials than those of normal cells,[80] potentially improving their efficacy as targeted anticancer agents. Moreover, as aforementioned, **Ir1**, **Rh1**, and **Ru1** showed much higher log P values than **Ir2**, **Rh2**, and **Ru2** which may improve their mitochondrial targeting ability. Generally, anticancer complexes with high lipophilicity can disrupt normal metabolic homeostasis and intracellular ROS levels by increasing their interaction with mitochondrial membranes.[81]

The biodistribution of **Ir1** in different subcellular compartments of A549 and BEAS-2B cells was quantitatively analyzed using ICP-MS.[82−84] After 48 h of exposure to **Ir1**, the iridium content in the mitochondria, cytoplasm (without mitochondria), and nucleus fractions isolated from A549 and BEAS-2B cells was measured (Figure 5). The results revealed that the majority of iridium was localized and accumulated in the mitochondrial fraction of both A549 and BEAS-2B cells. Furthermore, **Ir1** showed a higher accumulation in the mitochondria of A549 cells compared to normal cells. These observations are consistent with the observations from the aforementioned cellular localization experiments, further elucidating the mitochondrial targeting behavior of these complexes.

Laser confocal microscopy was also utilized to investigate how complexes **Ir1**, **Rh1**, and **Ru1** enter cells. Confocal microscopy images captured at λ_{ex} = 405 nm and 37 °C revealed that after 1 h of incubation, **Ir1**, **Rh1**, and **Ru1**

https://doi.org/10.1021/acs.inorgchem.4c03975
Inorg. Chem. 2024, 63, 24736−24753

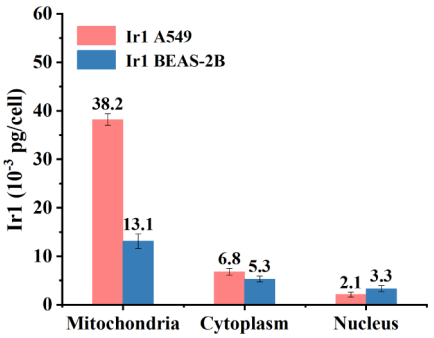

Figure 5. Subcellular distribution of iridium in A549 and BEAS-2B cells after incubation with **Ir1**(10 mM) for 1 h. The amount of iridium in mitochondrial, cytoplasmic, and nuclear fractions is measured by ICP-MS. Data were collected at least 3 times independently.

successfully penetrated A549 cells, as evidenced by speckled green fluorescence within the cytoplasm (Figure 6). It is widely recognized that small-molecule drugs can enter cells via either energy-independent or energy-dependent pathways.[81] Compared to the control group maintained at 37 °C, the fluorescence intensity in A549 cells incubated with **Ir1**, **Rh1**, or **Ru1** at a low temperature (4 °C) or pretreated with carbonyl cyanide 3-chlorophenylhydrazone (CCCP, a metabolic inhibitor) decreased significantly. This suggests that the uptake of **Ir1**, **Rh1**, and **Ru1** is energy-dependent. Additionally, no significant differences were observed when comparing A549 cells treated with the endocytosis inhibitor chloroquine to untreated cells, suggesting that endocytosis is not the primary uptake pathway for these complexes.

2.8. Mitochondrial Membrane Depolarization. Due to the selective accumulation of these complexes in mitochondria, their potential effects on mitochondrial functionality were also explored. The mitochondrial membrane potential (MMP, $\Delta\psi_m$) represents the electrical gradient essential for cellular functions, with a voltage difference across the mitochondrial membrane.[85] Mitochondrial damage and the loss of this membrane potential are key early events in the initiation of the apoptotic cascade. These disruptions initiate a series of biochemical changes within the mitochondrial membrane that lead to apoptosis.[86] We employed the JC-1 probe and flow cytometry to assess changes in the MMP of A549 cells and BEAS-2B cells incubated with complexes **Ir1** and **Ir2**. JC-1 is a widely utilized fluorescent probe that is ideal for detecting MMP due to its color-changing properties. In a high membrane potential environment, JC-1 aggregates in the mitochondrial matrix, forming J-aggregates that emit red fluorescence. Conversely, when the membrane potential is low, JC-1 exists as a monomer and emits green fluorescence, allowing for the easy detection of decreases in membrane potential through the shift from red to green fluorescence.[87,88] The results are expressed as the red/green fluorescence intensity ratio. In addition, we used CCCP (carbonyl cyanide *m*-chlorophenyl hydrazone) as a positive control. CCCP is a well-established mitochondrial uncoupler that disrupts MMP by allowing protons to flow across the mitochondrial membrane, thus, reducing the membrane potential. A549 cells were exposed to **Ir1** and **Ir2** at concentrations of 0.25, 0.5, and 1.0 × IC_{50} (Figure 7). **Ir1** caused a substantial decrease in MMP in A549 cancer cells relative to untreated cells. Specifically, as the concentration of **Ir1** increased from 0.25 × IC_{50} to 1 × IC_{50}, the percentage of cells with mitochondrial membrane depolarization rose by 58.7%, from 26.4% to 85.1% (Figure 7a). For comparison, treatment with **Ir2** in A549 cells and **Ir1** in BEAS-2B normal cells resulted in only minor changes in mitochondrial membrane depolarization, at 11.6% and 17.9%, respectively (Figure 7b,c). These findings align closely with the cytotoxicity and anticancer selectivity observed in these complexes. Specifically, complex **Ir1** demonstrated higher cytotoxicity and selective toxicity toward A549 cancer cells compared to BEAS-2B normal cells. Moreover, **Ir1** also exhibited greater cytotoxicity against both A549 and Hela cancer cells compared to that of **Ir2**. Therefore, the incorporation of the triphenylphosphine moiety in these complexes may enhance their anticancer efficacy through the mitochondrial pathway, specifically by targeting mitochondria and disrupting their normal function.

2.9. Cellular ROS Determination. The generation of intracellular ROS is closely linked to mitochondrial function.[89] Numerous studies have demonstrated that impaired mitochondria fail to regulate ROS production efficiently, leading to increased oxidative stress in cancer cells.[90] Since cancer cells typically endure heightened oxidative stress compared to normal cells, any additional increase in ROS levels induced by anticancer complexes tends to have a less pronounced effect on the redox balance in normal cells, potentially underpinning the selectivity of these agents.[91,92] Motivated by observations that

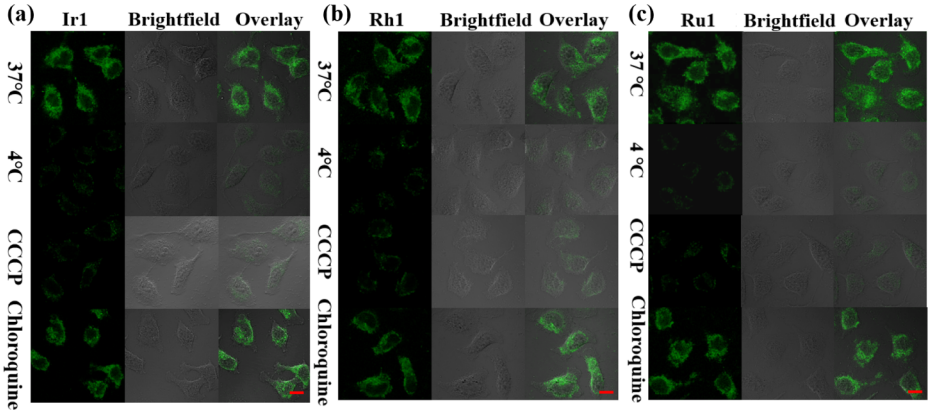

Figure 6. Effects of temperatures (37 or 4 °C), chloroquine (50 μM) and CCCP (50 μM) on cellular uptake of **Ir1** (2 μM) (a), **Ru1** (2 μM) (b), and **Rh1** (2 μM) (c). Scale bar: 20 μm.

https://doi.org/10.1021/acs.inorgchem.4c03975
Inorg. Chem. 2024, 63, 24736−24753

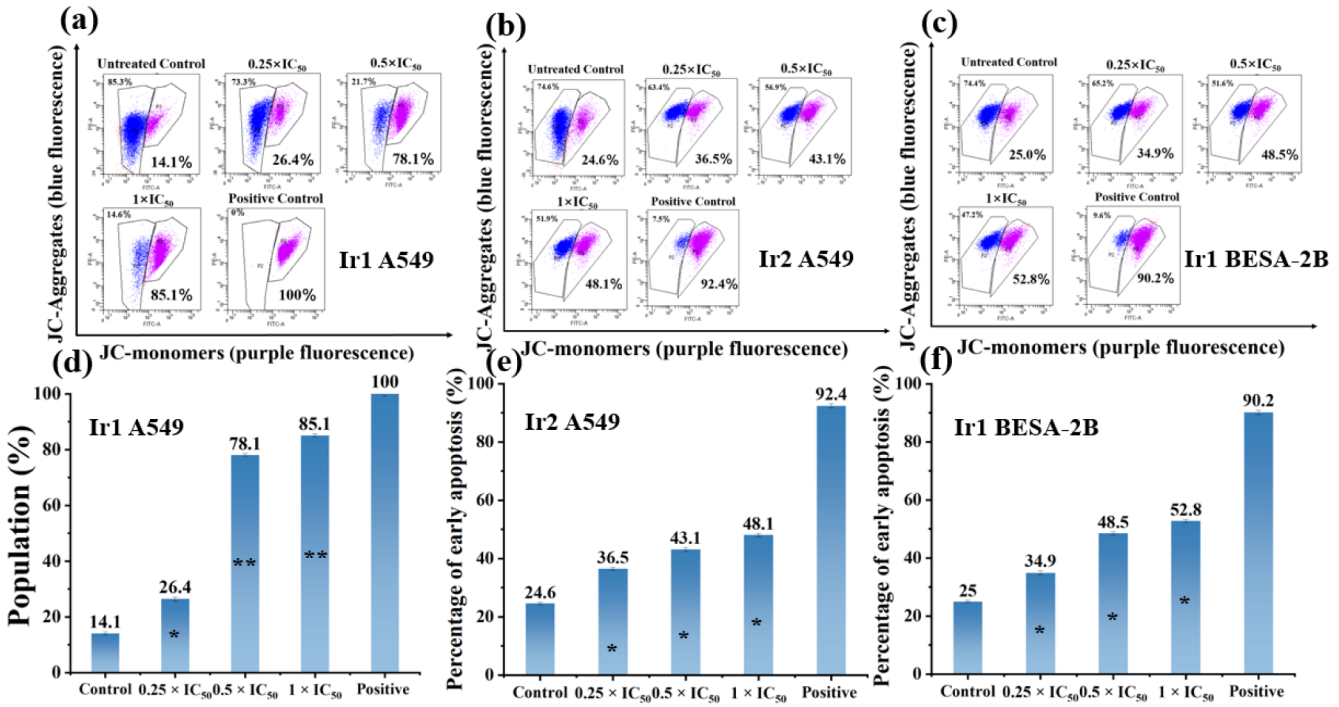

Figure 7. (a,d) Changes in the mitochondrial membrane potential of A549 cancer cells induced by **Ir1**. (b,e) Changes in the mitochondrial membrane potential of A549 cancer cells induced by **Ir2**. (c,f) Changes in the mitochondrial membrane potential of BEAS-2B cells induced by **Ir1.** CCCP (carbonyl cyanide *m*-chlorophenyl hydrazone) was used as a positive control to induce mitochondrial membrane depolarization. Data are quoted as mean ± SD of three replicates. p-Values were calculated after a test against the untreated control data, $*p < 0.05$, $**p < 0.01$.

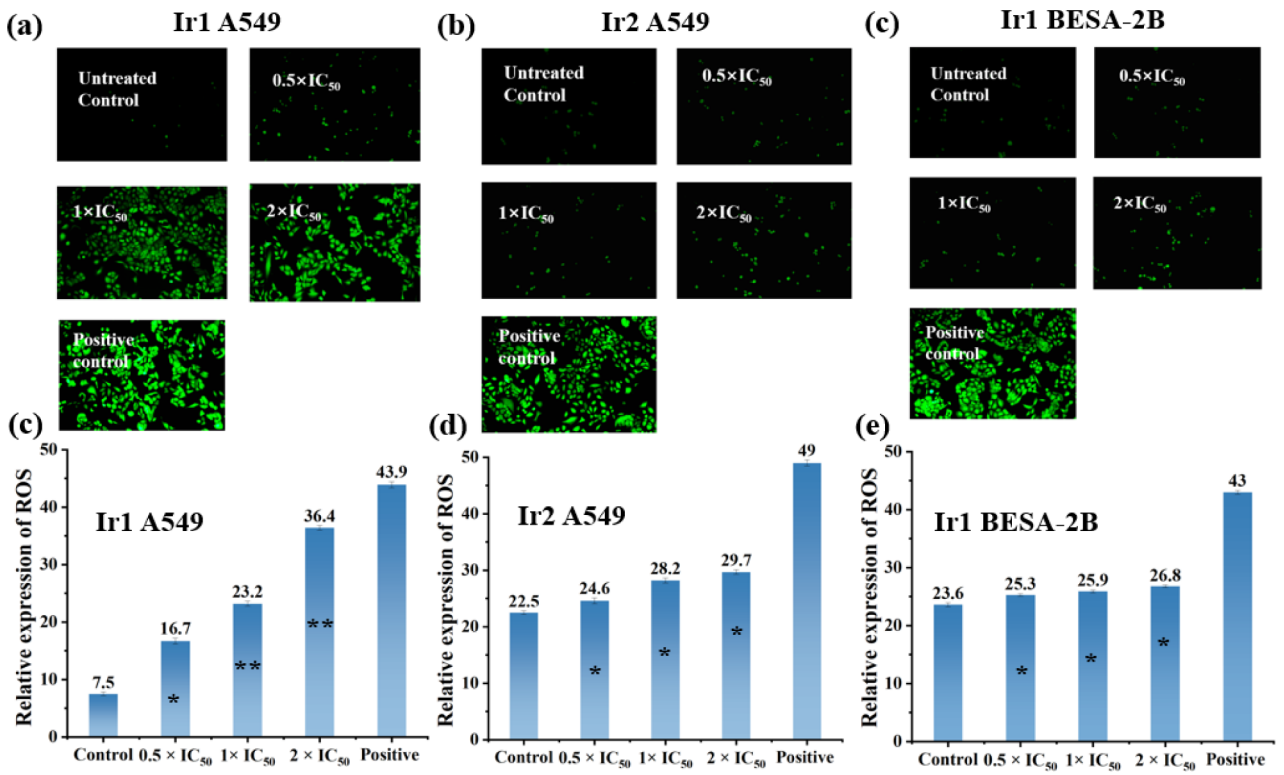

Figure 8. Analysis of ROS levels by fluorescence microscope after A549 cells were treated with **Ir1** (a,d) and **Ir2** (b,e) for 24 h at 37 °C. Analysis of ROS levels by fluorescence microscope after BESA-2B cells were treated with **Ir1** (c,f) for 24 h at 37 °C. Stained with DCFH-DA. ROSup was used as a positive control to induce reactive oxygen species (ROS) production. Data are quoted as mean ± SD of three replicates. *p*-Values were calculated after a test against the untreated control data, $*p < 0.05$, $**p < 0.01$.

some half-sandwich complexes, which are capable of either targeting mitochondria or promoting the oxidation of NADH to NAD^+, also elevate ROS levels in cancer cells,[44] we measured ROS levels in A549 cells and BEAS-2B cells exposed

https://doi.org/10.1021/acs.inorgchem.4c03975
Inorg. Chem. 2024, 63, 24736−24753

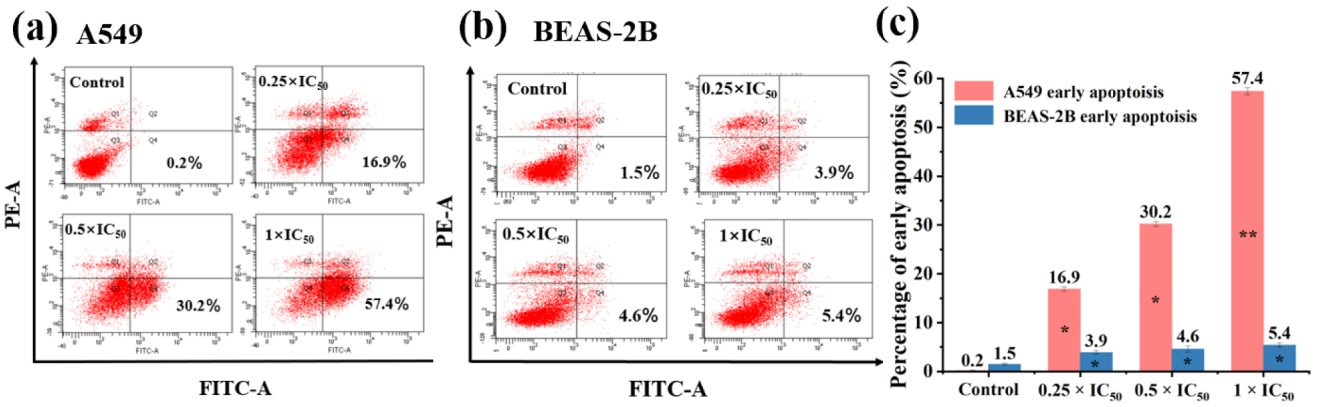

Figure 9. (a) Apoptosis analysis for A549 cells after treatment with complex **Ir1** at the concentrations of 0.25 × IC_{50}, 0.5 × IC_{50}, and 1 × IC_{50} for 48 h. (b) Apoptosis analysis for BEAS-2B cells after treatment with complex **Ir1** at the concentrations of 0.25 × IC_{50}, 0.5 × IC_{50}, and 1 × IC_{50} for 48 h. (c) Histograms of apoptosis analysis for A549 and BEAS-2B cells after treatment with complex **Ir1** at the concentrations of 0.25 × IC_{50}, 0.5 × IC_{50}, and 1 × IC_{50} for 48 h. Positive control was treated with cisplatin (Figures S52 and S53). Data are quoted as the mean ± standard deviation (SD) of three replicates. *p*-Values were calculated after a test against the untreated control data, *$p < 0.05$, **$p < 0.01$.

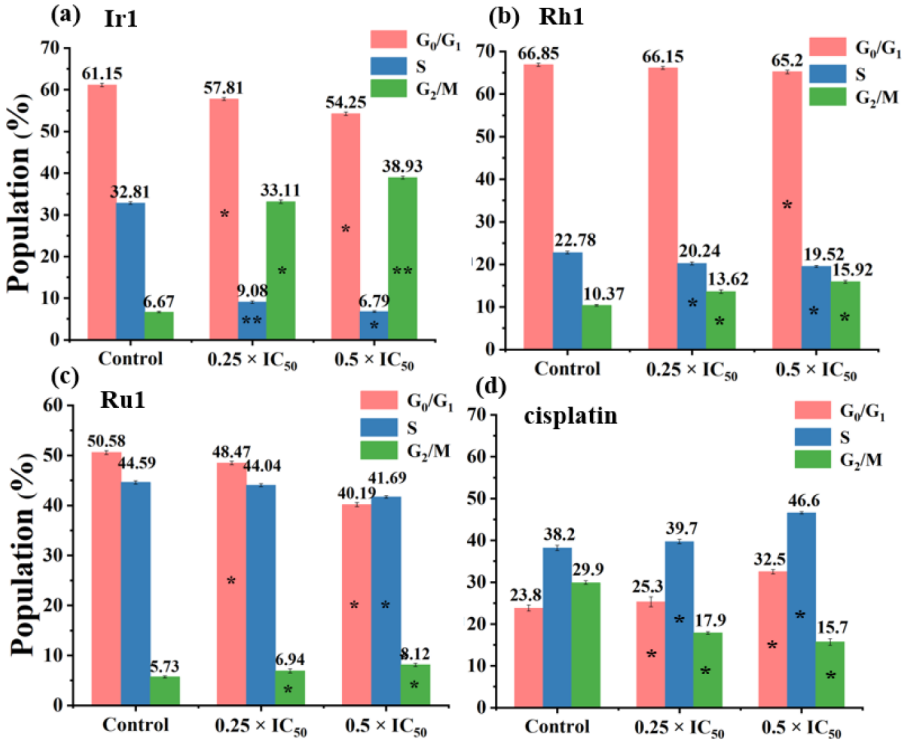

Figure 10. Flow cytometry data for cell cycle distribution of A549 cancer cells exposed to **Ir1** (a), **Rh1** (b), **Ru1** (c), and cisplatin (d) for 24 h. Concentrations used were 0.25 × IC_{50} and 0.5 × IC_{50}. Cell staining for flow cytometry was carried out using PI/RNase. Data are quoted as mean ± standard deviation (SD) of three replicates. *p*-Values were calculated after a test against the untreated control data, *$p < 0.05$, **$p < 0.01$.

to various concentrations of complexes **Ir1** and **Ir2** (Figure 8). The measurements were performed by using a fluorescence microscope with DCFH-DA as the probe. This assay assesses overall oxidative stress rather than identifying specific ROS. In comparison to the untreated control cells, there is a noticeable concentration-dependent rise in fluorescence intensity. The level of ROS (36.4%) at the concentration of 2 × IC_{50} was on par with the positive control treated with ROSup, indicating elevated ROS levels, was observed in A549 cells treated with complex **Ir1**, suggesting that these complexes may disrupt the intracellular redox through the generation of ROS. However, the fluorescence intensity in A549 cells, indicative of ROS levels, was lower for **Ir2** compared to **Ir1** at the same concentrations, and no obvious concentration-dependent increase was observed. Furthermore, only minimal changes in ROS levels were detected in BEAS-2B cells despite increasing concentrations of **Ir1**. These results are consistent with the demonstrated cytotoxicity and anticancer selectivity of the complexes in this system. Notably, several previously reported half-sandwich complexes have been shown to generate ROS through catalytic hydride transfer from NADH to O_2.[61,76] Given that we have observed the catalytic transfer of NADH to NAD^+ with these complexes in this system, it is plausible that the induction of ROS could also be related to the oxidation of NADH to NAD^+. However, since targeting mitochondria and disrupting mitochondrial membrane potential (MMP) also

https://doi.org/10.1021/acs.inorgchem.4c03975
Inorg. Chem. 2024, 63, 24736−24753

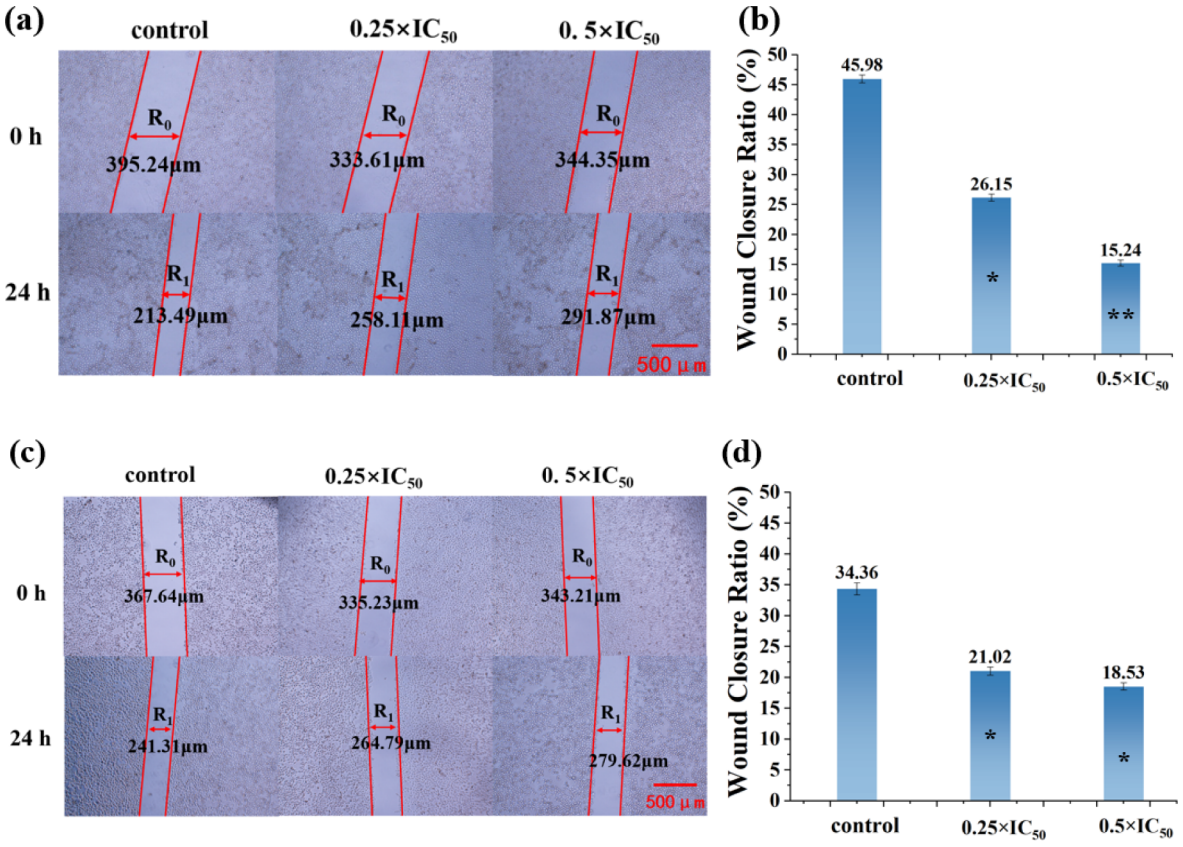

Figure 11. (a) Wound-healing assay for A549 cells treated with **Ir1** for 24 h. (b) Histograms analysis for A549 cells treated with **Ir1** for 24 h; typical images were taken at 0 and 24 h. (c) Wound-healing assay for A549 cells treated with cisplatin for 24 h. (d) Histograms analysis for A549 cells treated with cisplatin for 24 h; typical images were taken at 0 and 24 h. The widths of the wounds are indicated with lines (μm). Scale bar: 500 μm. Wound Closure Rate: $(R_0 - R_1)/R_0 \times 100\%$. Data are quoted as mean ± standard deviation (SD) of three replicates. p-Values were calculated after a test against the untreated control data, *$p < 0.05$, **$p < 0.01$.

impairs the effective regulation of ROS production, mitochondria-mediated ROS overproduction cannot be excluded. Regardless, the elevated levels of ROS can be considered one of MoAs for these complexes.

2.10. Apoptosis. Previous reports indicate that anticancer complexes generating high ROS levels can disrupt cellular redox balance, thereby inducing apoptosis and cellular damage.[93,94] The apoptosis-inducing mechanism of cell death was investigated by using the annexin V/PI assay. A549 cells were treated with **Ir1**, **Rh1**, **Ru1**, and cisplatin as a positive control at concentrations of 0.25, 0.5, and 1 × IC_{50} for 48 h, and analyzed via flow cytometry (Figure 9). A concentration-dependent rise in early apoptotic cell populations was observed for these complexes (Figures 9a,b, S50−S53). To validate the assay's reliability, cisplatin was used as a comparison, as it is known to induce apoptosis in cancer cells. For example, when A549 cells were treated with **Ir1**, **Rh1**, **Ru1**, and cisplatin at a concentration of 1 × IC_{50}, the percentages of cells undergoing early apoptosis were 57.4%, 96.1%, 51.7%, and 16.1%, respectively. Notably, cisplatin induces both early and late apoptosis in A549 and BEAS-2B cells (Figures S52 and S53), reflecting its dual-phase apoptotic effect. In contrast, the complexes in this system primarily trigger early apoptosis, suggesting a mechanistic difference. However, the results for cisplatin confirmed the effectiveness of the experimental setup, thereby strengthening the reliability of the observed apoptotic effects induced by **Ir1**, **Rh1**, and **Ru1**. In contrast, when BEAS-2B normal cells were treated with **Ir1** under the same conditions, only a marginal increase in early apoptotic cells was observed, ranging from 3.9% to 5.4% (Figure 9b,c). Specifically, at a 1 × IC_{50} concentration of **Ir1**, early apoptosis occurred in just 5.4% of BEAS-2B cells, a minimal change from that in the untreated group. This selective induction of apoptosis aligns with the observed low cytotoxicity of **Ir1** toward BEAS-2B normal cells, suggesting that these complexes preferentially target cancer cells while sparing normal cells.

Active caspase-3 is a key effector in multiple apoptotic pathways, making it an effective marker for detecting apoptotic cells via flow cytometry.[95] After treatment with **Ir1** at 0.5× IC_{50} and 1× IC_{50} concentrations for 24 h, 19.5% and 30.9% of active caspase 3-positive A549 cells were determined, respectively. These percentages were significantly higher than the 9.77% observed in untreated cells (Figure S54), further indicating that these complexes induce cell death primarily through the apoptotic pathway.

2.11. Cell-Cycle Arrest. Cell cycle arrest, often triggered by apoptotic signals, is closely linked to the acceleration of apoptosis. Many anticancer complexes induce apoptosis by impeding the cell cycle.[96] The impact of **Ir1**, **Rh1**, and **Ru1** on cell cycle arrest in A549 cancer cells was investigated by using flow cytometry. Treatment with these complexes at concentrations of 0.25 × IC_{50} and 0.5 × IC_{50} for 24 h resulted in a concentration-dependent rise in the cell population at the G_2/M phase, along with a decrease in the S and G_0/G_1 phases (Figures 10a−c and S55−S57). Specifically, at a concentration of 0.5 × IC_{50}, the proportion of A549 cells in the G_2/M phase

https://doi.org/10.1021/acs.inorgchem.4c03975
Inorg. Chem. 2024, 63, 24736−24753

increased by 32.26%, 5.55%, and 2.39% for **Ir1**, **Rh1**, and **Ru1**, respectively, compared to the untreated group. Cisplatin was used as a comparison for cell cycle analysis, primarily causing cell cycle arrest in the G_0/G_1 and S phases (Figures 10d and S58). This arrest pattern differs from that induced by the complexes in this system, indicating distinct mechanisms of biological action between these two metal-based compounds. Consequently, **Ir1**, **Rh1**, and **Ru1** were able to induce cell cycle perturbations, leading to arrest in the G_2/M phase. Notably, despite differences in the metal centers (iridium^{III}, rhodium^{III}, and ruthenium^{II}), all complexes consistently induced early apoptosis, indicating that early apoptosis induction was not influenced by the type of metal center.

2.12. Inhibition of Cell Migration. Tumor metastasis represents a grave aspect of malignancy, and repeated cell migration can lead to dire outcomes, often underlying the intractability of tumors.[97] Understanding how antitumor drugs block metastasis is essential for developing new treatments that enhance the body's antimetastatic capabilities. **Ir1** was selected for further metastasis studies due to its high cytotoxicity and superior selectivity. A wound-healing assay was conducted to investigate the effects of **Ir1** on inhibiting the migration of A549 cancer cells (Figure 11a,b). The results showed a significant reduction in the wound closure rate (WCR) for cells treated with complex **Ir1** at 0.5 × IC_{50}, decreasing from 45.98% in the untreated control to 15.24%. For comparison, the WCR of cells treated with cisplatin, used as a positive control at 0.5 × IC_{50}, decreased from 34.36% in the control group to 18.53% (Figures 11c,d). Additionally, **Ir1** demonstrated a dose-dependent decrease in the WCR of A549 cancer cells, indicating that complex **Ir1** was effective at curtailing the in vitro migration of A549 cancer cells.

3. CONCLUSIONS

In summary, this study successfully synthesized and characterized novel triphenylphosphine-modified half-sandwich iridium^{III}, rhodium^{III}, and ruthenium^{II} complexes. These complexes exhibit potent cytotoxicity against A549 and HeLa cancer cell lines, notably surpassing that of comparative complexes lacking a triphenylphosphine moiety. Most importantly, they also demonstrate improved selectivity toward cancer cells over normal BEAS-2B cells with high selectivity index. The enhanced anticancer efficacy of these complexes is attributed primarily to their ability to target mitochondria and disrupt mitochondrial function, as confirmed through confocal microscopy and flow cytometry. These complexes effectively depolarize mitochondrial membrane potential, increase ROS production, and trigger intrinsic apoptosis pathways. Additionally, they induce cell cycle arrest at the G_2/M phase and present significant potential to prevent metastasis. Overall, the use of triphenylphosphine-modified complexes to target mitochondria presents a potential approach for developing anticancer agents with enhanced efficacy and reduced side effects.

4. EXPERIMENTAL SECTION

L2 was synthesized following methods from the literature.[98] **D1−D3** were obtained using previously reported procedures[51,53] General considerations and detailed experimental procedures for biological assays are provided in the Supporting Information.

4.1. Synthesis of Ligands. L1: (4-(4-formylphenyl)butyl) triphenylphosphine bromide were synthesized by reference method. A mixture of 1,10-phenanthroline-5,6-dione (0.210 g, 1.0 mmol), (4-(4-formylphenyl)butyl) triphenylphosphine bromide (0.518 g, 1.0 mmol), ammonium acetate (1.734 g, 22.5 mmol), and ethanol (30 mL) was refluxed at 85 °C for 24 h. After reaction solution was cooled, added KPF_6 saturation solution to give a brown precipitate. Filter, wash with water, and dry to obtain a brown powder. Yield, 0.318 g (45%). This compound is previously known. ^{1}H NMR (DMSO-d_6, 500 MHz) δ 13.66 (s, 1H), 9.03 (d, J = 3.9 Hz, 2H), 8.96 (d, 1H), 8.91 (d, 1H), 8.24 (d, 2H), 7.92 (t, 3H), 7.87 (m, 14H), 7.13 (d, 2H), 4.16 (t, 2H, OCH_2), 3.78 (m, 2H, CH_2CH_2), 2.03 (m, 2H, CH_2CH_2), 1.82 (m, 2H, PCH_2). ^{13}C NMR (DMSO-d_6, 126 MHz): δ 160.15 (C-O), 151.25 (C═N), 148.03, 135.43, 134.03, 130.77, 130.27, 128.28 (C-N), 123.86 (C-NH), 123.07, 119.30, 119.06, 118.62, 118.38), 115.42, 66.65 (OCH_2), 29.58 (OCH_2CH_2), 20.03 (PCH_2), 18.97 (PCH_2CH_2). ^{31}P NMR (202 MHz, DMSO-d_6): δ 24.08, −137.16, −140.67, −144.18, −147.70, −151.21.

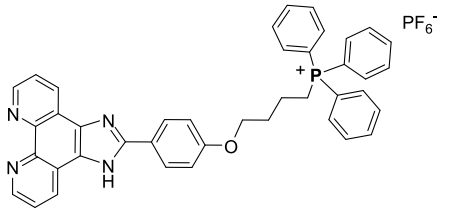

4.2. Synthesis of Complexes. *4.2.1. General Procedures.* Synthesis of iridium^{III}, rhodium^{III}, and ruthenium ^{II} complexes: A mixture of bimetallic precursors (**D1−D3**) (1 equiv), ligands (**L1−L2**) (2 equiv), and NH_4PF_6 (2 equiv) in CH_2Cl_2/CH_3OH (v/v, approximately 1:1) was stirred at ambient temperature for 24 h. Afterward, the solvents were evaporated by using a rotary evaporator. The resulting solid was dissolved in CH_2Cl_2 and filtered. The filtrate was subsequently concentrated, and the residue was recrystallized from CH_2Cl_2 and hexane to yield a pale yellow powder.

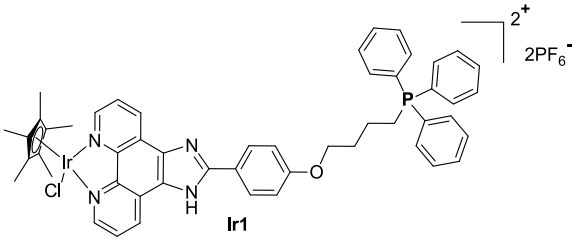

Ir1

Ir1: (69 mg, Yield 54%). ^{1}H NMR (DMSO-d_6, 500 MHz) δ 14.24 (s,1H, N*H*), 9.32 (s, 2H), 9.24 (d, 2H), 8.27 (d, 4H), 7.92 (t, 3H), 7.88 (m, 13H), 7.18 (d, 2H), 4.18 (t, 2H, OCH_2), 3.70 (m, 2H CH_2CH_2), 1.99 (m, 2H, CH_2CH_2), 1.78 (d, 2H, PCH_2), 1.73 (s, 15H, Cp*-CH_3). ^{13}C NMR (DMSO-d_6, 126 MHz) δ 160.75 (C-O), 153.47, 150.36 (C═N), 144.32, 135.43 (P-Ph_3), 134.07 (P-Ph_3), 133.22, 130.77 (P-Ph_3), 128.77 (C-N), 127.83 (C-NH), 122.34, 119.30, 118.62, 115.62, 89.62, 66.87 (OCH_2), 29.58 (OCH_2CH_2), 20.11 (p-CH_2), 18.95 (p-CH_2CH_2), 8.68 (Cp*-CH_3). ESI-MS (m/z): calcd for $C_{51}H_{48}ClIrN_4OP$ 991.2884, found 991.2811 [M−H−$2PF_6$]$^+$. ^{31}P NMR (202 MHz, DMSO-d_6): δ 24.07, −133.65, −137.17, −140.68, −144.19, −147.71, −151.22, −154.73. Elemental analysis: calcd for $C_{51}H_{49}ClIrN_4OP_3F_{12}$: C, 47.76; H, 3.85; N, 4.37, found: C, 48.01; H, 3.67; N, 4.21.

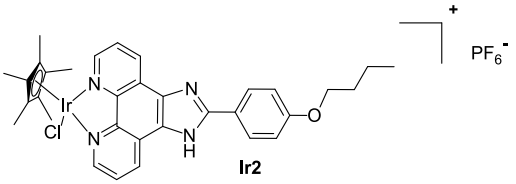

Ir2

Ir2: (65 mg, Yield 70%). ^{1}H NMR (DMSO-d_6, 500 MHz) δ 14.23 (s, 1H, N*H*), 9.32 (s, 2H), 9.25 (s, 2H), 8.35 (m, 4H), 7.23 (d, 2H), 4.12 (t, 2H, OCH_2), 1.78 (d, 2H, CH_2CH_2), 1.78 (m, 15H, Cp*−CH_3), 1.49 (m, 2H, CH_2CH_2), 0.98 (t, 3H, CH_2CH_3). ^{13}C NMR (DMSO-d_6, 126 MHz) δ 161.10 (C-O), 153.67, 150.63 (C═N), 150.39, 145.45, 144.29, 133.78, 133.24, 128.83 (C-N), 127.80 (C-

https://doi.org/10.1021/acs.inorgchem.4c03975
Inorg. Chem. 2024, 63, 24736−24753

NH), 115.60, 89.60, 68.02 (OCH_2), 31.16 (OCH_2CH_2), 19.20 (CH_2CH_3), 14.21 (CH_2CH_3), 8.70 (Cp*-CH_3), 8.18 (Cp*-CH_3). ESI-MS (m/z): calcd for $C_{33}H_{35}ClIrN_4O$ 731.2129, found 731.2124 $[M-PF_6]^+$. Elemental analysis: calcd for:$C_{33}H_{35}ClIrN_4OPF_6$: C, 45.23; H, 4.03; N, 6.39, found: C, 45.52; H, 3.86; N, 6.12.

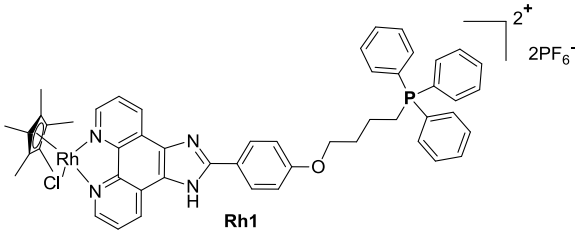

Rh1

Rh1: (68 mg Yield 58%). ^{1}H NMR (DMSO-d_6, 500 MHz) δ 9.33 (m, 2H), 9.24 (d, 2H), 8.24 (m, 3H), 7.92 (m, 3H), 7.86 (m, 13H), 7.18 (d, 2H), 4.18 (t, 2H, OCH_2), 3.71 (m, 2H, CH_2CH_2), 1.99 (m, 2H, CH_2CH_2), 1.83 (m, 2H, PCH_2), 1.76 (d, 15H, Cp*-CH_3). ^{13}C NMR (DMSO-d_6, 126 MHz) δ 160.76 (C-O), 153.19 (C═N), 150.66, 143.12, 135.42, 134.07, 133.01, 130.75, 128.69, 127.43, 122.25, 119.30, 118.62, 115.64, 99.29, 97.44, 66.84 (OCH_2), 29.73 (OCH_2CH_2), 20.53 (p-CH_2CH_2), 20.13 (P-CH_2CH_2), 8.99 (Cp*-CH_3). ^{31}P NMR (202 MHz, DMSO-d_6): δ 24.07, −137.17, −140.68, −144.19, −147.71, −151.22. ESI-MS (m/z): calcd for $C_{51}H_{48}ClRhN_4OP$ 901.2309, found 901.2297, $[M-H-2PF_6]^+$. Elemental analysis: calcd for $C_{51}H_{49}ClRhN_4OP_3F_{12}$: C, 51.34; H, 4.14; N, 4.70, found:C, 51.59; H, 3.92; N, 4.46

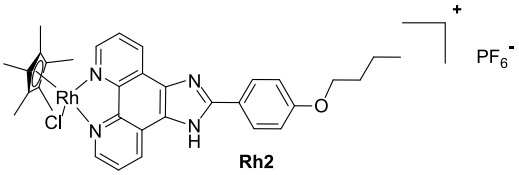

Rh2

Rh2: (60 mg Yield 71%). ^{1}H NMR (DMSO-d_6, 500 MHz) δ 9.30 (d, 2H), 9.26 (d, 2H), 8.32 (m, 4H), 7.20 (d, 2H), 4.10 (t, 2H, OCH_2), 1.82 (m, 2H, CH_2CH_2), 1.77 (s, 15H, Cp*-CH_3), 1.49 (m, 2H, CH_2CH_2), 0.98 (t, 3H, CH_2CH_3). ^{13}C NMR (DMSO-d_6, 126 MHz) δ 160.85 (C-O), 154.53, 148.28 (C═N), 129.22, 126.29 (C-NH), 121.99, 114.86, 96.82, 67.85 (OCH_2), 31.23 ($CH_2CH_2CH_2$), 19.22 (CH_2CH_3), 13.85 (CH_2CH_3), 9.10 (Cp*-CH_3). ESI-MS (m/z): calcd for $C_{33}H_{35}ClIrN_4O$ 641.1788, found 605.1780 $[M-PF_6]^+$. Elemental analysis: calcd for $C_{33}H_{35}ClIrN_4OPF_6$: C, 50.36; H, 4.48; N, 7.12. found: C, 50.52; H, 4.26; N, 6.96.

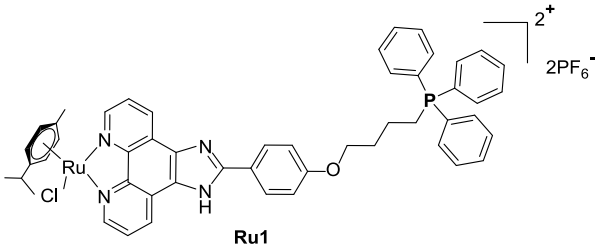

Ru1

Ru1: (56 mg Yield 48%). ^{1}H NMR (DMSO-d_6, 500 MHz) δ 14.16 (s, 1H, NH), 9.86 (d, 2H), 9.20 (d, 2H), 8.24 (d, 3H), 8.19 (s, 1H), 7.92 (t, 3H), 7.87 (m, 13H), 7.17 (d, 2H), 6.34 (d, 2H), 6.11 (d, 2H), 4.17 (t, 2H), 3.74 (m, 2H), 2.65 (m, 1H, $CH(CH_3)_2$), 2.21 (s, 3H, CCH_3), 2.02 (m, 2H), 1.77 (m, 2H), 0.90 (d, 6H, $CH(CH_3)_2$). ^{13}C NMR (DMSO-d_6, 126 MHz) δ 160.74 (C-O), 154.16, 153.35 (C═N), 143.46, 135.44 (P-Ph_3), 134.03, 132.67, 130.78 (P-Ph_3), 128.66, 126.68, 122.31 (C-NH), 119.31 (C-N), 118.62, 115.62, 104.44, 103.47, 86.76, 85.98, 84.46, 66.80 (OCH_2), 30.89 ($CH(CH_3)_2$), 22.09 ($CH(CH_3)_2$), 20.51 (OCH_2CH_2), 20.10 (arene-CH_3), 18.96 (p-CH_2CH_2), 18.73 (P-CH_2CH_2). ^{31}P NMR (202 MHz, DMSO-d_6): δ 24.08, −133.65, −137.16, −140.68, −144.19, −147.70, −151.22. ESI-MS(m/z):calcd for $C_{51}H_{48}ClRuN_4OP_2F_6$ 1045.1940, found 1045.1916, $[M-PF_6]^+$. Elemental analysis: calcd for $C_{51}H_{48}ClRuN_4OP_3F_{12}$: C, 51.46; H, 4.06; N, 4.71, found: C, 51.59; H, 3.91; N, 4.44.

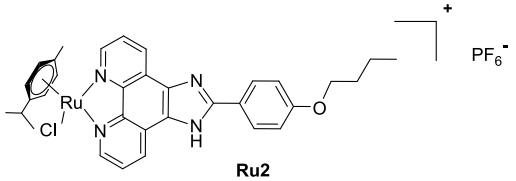

Ru2

Ru2: (57 mg Yield 68%). ^{1}H NMR (DMSO-d_6, 500 MHz) δ 14.25 (s, 1H, NH), 9.86 (d, 2H), 9.24 (d, 2H), 8.26 (d, 2H), 8.25 (d, 2H), 7.21 (d, 2H), 6.34 (d, 2H), 6.12 (d, 2H), 4.11 (t, 2H), 2.62 (m, 1H, $CH(CH_3)_2$), 2.21 (s, 3H, CCH_3), 1.76 (m, 2H), 1.49 (m, 2H), 0.98 (t, 3H, CH_2CH_3), 0.91 (d, 6H, $CH(CH_3)_2$). ^{13}C NMR (DMSO-d_6, 126 MHz) δ 160.99 (C-O), 154.04, 153.42 (C═N), 143.43, 132.68, 128.65, 126.64 (C-N), 122.09 (C-NH), 115.55, 104.42, 103.4, 86.83, 86.66, 85.97, 84.45, 67.97 (OCH_2), 31.18 ($CH(CH_3)_2$), 30.89 (CH_2), 22.31 ($CH(CH_3)_2$), 19.20 (arene-CH_3), 18.72 (CH_2CH_3), 14.17 (CH_2CH_3).ESI-MS (m/z): calcd for $C_{33}H_{34}ClRuN_4O$ 639.1465, found 639.1464, $[M-PF_6]^+$. Elemental analysis: calcd for $C_{33}H_{34}ClRuN_4OPF_6$: C, 50.55; H, 4.37; N, 7.51. found: C, 50.76; H, 4.21; N, 7.34.

■ ASSOCIATED CONTENT

Supporting Information

The Supporting Information is available free of charge at https://pubs.acs.org/doi/10.1021/acs.inorgchem.4c03975.

Additional experimental details and methods, ^{1}H, ^{31}P, and ^{13}C{^{1}H} NMR spectra, and ESI-MS spectra for all compounds (PDF)

■ AUTHOR INFORMATION

Corresponding Authors

Zhe Liu − *Key Laboratory of Life-Organic Analysis of Shandong Province, Key Laboratory of Green Natural Products and Pharmaceutical Intermediates in Colleges and Universities of Shandong Province, School of Chemistry and Chemical Engineering, Qufu Normal University, Qufu 273165, P. R. China*; orcid.org/0000-0001-5796-4335; Email: liuzheqd@163.com

Lihua Guo − *Key Laboratory of Life-Organic Analysis of Shandong Province, Key Laboratory of Green Natural Products and Pharmaceutical Intermediates in Colleges and Universities of Shandong Province, School of Chemistry and Chemical Engineering, Qufu Normal University, Qufu 273165, P. R. China*; orcid.org/0000-0002-0842-9958; Email: guolihua@qfnu.edu.cn

Authors

Hanxiu Fu − *Key Laboratory of Life-Organic Analysis of Shandong Province, Key Laboratory of Green Natural Products and Pharmaceutical Intermediates in Colleges and Universities of Shandong Province, School of Chemistry and Chemical Engineering, Qufu Normal University, Qufu 273165, P. R. China*

Heqian Dong − *Key Laboratory of Life-Organic Analysis of Shandong Province, Key Laboratory of Green Natural Products and Pharmaceutical Intermediates in Colleges and Universities of Shandong Province, School of Chemistry and Chemical Engineering, Qufu Normal University, Qufu 273165, P. R. China*

Kangning Lai − *Key Laboratory of Life-Organic Analysis of Shandong Province, Key Laboratory of Green Natural Products and Pharmaceutical Intermediates in Colleges and Universities of Shandong Province, School of Chemistry and Chemical Engineering, Qufu Normal University, Qufu 273165, P. R. China*

https://doi.org/10.1021/acs.inorgchem.4c03975
Inorg. Chem. 2024, 63, 24736−24753

Zhihao Yang − *Key Laboratory of Life-Organic Analysis of Shandong Province, Key Laboratory of Green Natural Products and Pharmaceutical Intermediates in Colleges and Universities of Shandong Province, School of Chemistry and Chemical Engineering, Qufu Normal University, Qufu 273165, P. R. China*

Chunyan Fan − *Key Laboratory of Life-Organic Analysis of Shandong Province, Key Laboratory of Green Natural Products and Pharmaceutical Intermediates in Colleges and Universities of Shandong Province, School of Chemistry and Chemical Engineering, Qufu Normal University, Qufu 273165, P. R. China*

Yuting Luo − *Key Laboratory of Life-Organic Analysis of Shandong Province, Key Laboratory of Green Natural Products and Pharmaceutical Intermediates in Colleges and Universities of Shandong Province, School of Chemistry and Chemical Engineering, Qufu Normal University, Qufu 273165, P. R. China*

Wenting Qin − *Key Laboratory of Life-Organic Analysis of Shandong Province, Key Laboratory of Green Natural Products and Pharmaceutical Intermediates in Colleges and Universities of Shandong Province, School of Chemistry and Chemical Engineering, Qufu Normal University, Qufu 273165, P. R. China*

Complete contact information is available at: https://pubs.acs.org/10.1021/acs.inorgchem.4c03975

Notes

The authors declare no competing financial interest.

■ ACKNOWLEDGMENTS

The authors thank the Taishan Scholars Program, the Natural Science Foundation of Shandong Province (ZR2022MB038), the Young Talents Invitation Program of Shandong Provincial Colleges and Universities for support, and the Shiyanjia Lab (https://www.shiyanjia.com) for the mass spectrum test.

■ REFERENCES

(1) Florea, A. M. D.; Büsselberg. Cisplatin as an anti-tumor drug: cellular mechanisms of activity, drug resistance and induced side effects. *Cancers* **2011**, *3*, 1351−1371.

(2) Wang, X.; Wang, X.; Jin, S.; Muhammad, N.; Guo, Z. Stimuli-responsive therapeutic metallodrugs. *Chem. Rev.* **2019**, *119*, 1138−1192.

(3) Ho, G. Y.; Woodward, N.; Coward, J. I. Cisplatin versus carboplatin: comparative review of therapeutic management in solid malignancies. *Crit. Rev. Oncol. Hematol.* **2016**, *102*, 37−46.

(4) Oun, R.; Moussa, Y. E.; Wheate, N. J. The side effects of platinum-based chemotherapy drugs: a review for chemists. *Dalton Trans.* **2018**, *47*, 6645−6653.

(5) Peng, K.; Liang, B.-B.; Liu, W.; Mao, Z.-W. What blocks more anticancer platinum complexes from experiment to clinic: Major problems and potential strategies from drug design perspectives. *Coord. Chem. Rev.* **2021**, *449*, 214210.

(6) Muhammad, N.; Sadia, N.; Zhu, C.; Luo, C.; Guo, Z. X.; Wang. Biotin-tagged platinum(iv) complexes as targeted cytostatic agents against breast cancer cells. *Chem. Commun.* **2017**, *53*, 9971−9974.

(7) Zhang, D.; Zheng, Y.; Tan, C. P.; Sun, J. H.; Zhang, W.; Ji, L.; Mao, Z. Graphene oxide decorated with Ru(II)-polyethylene glycol complex for lysosome-targeted imaging and photodynamic/photothermal therapy. *ACS Appl. Mater. Interfaces* **2017**, *9*, 6761−6771.

(8) Xiong, X.; Liu, L.; Mao, Z.; Zou, T. Approaches towards understanding the mechanism-of-action of metallodrugs. *Coord. Chem. Rev.* **2022**, *453*, 214311−214339.

(9) Singh, D. Organelle Targeted Drug Delivery: Key Challenges, Recent Advancementsand Therapeutic Implications. *Endocr. Metab. Immune.* **2024**, *24*, 1480−1487.

(10) Sahu, P.; Agarwal, S.; Tomar, S.; Vyas, S.; Kashaw, S. K.; Rajoriya, V. Multifunctional Nanoparticles for Organelle-Specific Targeted Drug Delivery in Cancer Therapy. *Curr. Nanomed.* **2022**, *12*, 191−203.

(11) Shao, X.; Meng, C.; Song, W.; Zhang, T.; Chen, Q. Subcellular Visualization: Organelle-Specific Targeted Drug Delivery and Discovery. *Adv. Drug Delivery Rev.* **2023**, *199*, 114977−114977.

(12) Li, W.; Li, T.; Pan, Y.; Li, S.; Xu, G.; Zhang, Z.; Liang, H.; Yang, F. Designing a Mitochondria-Targeted Theranostic Cyclometalated Iridium(III) Complex: Overcoming Cisplatin Resistance and Inhibiting Tumor Metastasis through Necroptosis and Immune Response. *J. Med. Chem.* **2024**, *67*, 3843−3859.

(13) Ma, X.; Lin, N.; Yang, Q.; Liu, P.; Ding, H.; Xu, M.; Ren, F.; Shen, Z. Y.; Hu, K.; Meng, S.; Chen, H. Biodegradable copper-iodide clusters modulate mitochondrial function and suppress tumor growth under ultralow-dose X-ray irradiation. *Nat. Commun.* **2024**, *15* (1), 8092.

(14) Wang, B.; Hu, S.; Teng, Y.; Chen, J.; Wang, H.; Xu, Y. Z.; Wang, K. Y.; Xu, J. G.; Cheng, Y. Z.; Gao, X. Current advance of nanotechnology in diagnosis and treatment for malignant tumors. *Signal Transduction Targeted Ther.* **2024**, *9* (1), 200.

(15) Yang, Y.; Zou, X.; Sun, Y.; Chen, F.; Zhao, J.; Gou, S. Naphthalene Diimide-Functionalized Half-Sandwich Ru(II) Complexes as Mitochondria-Targeted Anticancer and Antimetastatic Agents. *Inorg. Chem.* **2023**, *62*, 9649−9660.

(16) Gupta, A.; Pandey, A. K.; Mondal, T.; Bhattacharya, J.; Sasmal, P. K. Multifunctional Iridium(III)−Platinum(IV) Conjugates as Potent Anticancer Theranostic Agents. *J. Med. Chem.* **2023**, *66*, 8687−8704.

(17) Singh, D. A sojourn on mitochondria targeted drug delivery systems for cancer: Strategies, clinical and future prospects. *Mitochondrion* **2024**, *74*, 101826.

(18) Murphy, M. P.; Hartley, R. C. Mitochondria as a therapeutic target for common pathologies. *Nat. Rev. Drug Discovery* **2018**, *17*, 865−886.

(19) Nuevo-Tapioles, C.; Santacatterina, F.; Stamatakis, K.; Núñez de Arenas, C.; Gómez de Cedrón, M.; Formentini, L.; Cuezva, J. M. Coordinate β-adrenergic inhibition of mitochondrial activity and angiogenesis arrest tumor growth. *Nat. Commun.* **2020**, *11* (1), 3606.

(20) Porporato, P. E.; Filigheddu, N.; Pedro, J. M. B.-S.; Kroemer; Galluzzi, L. Mitochondrial metabolism and cancer. *Cell Res.* **2018**, *28*, 265−280.

(21) Zorova, L. D.; Popkov, V. A.; Plotnikov, E. Y.; Silachev, D. N.; Pevzner, I. B.; Jankauskas, S. S.; Babenko, V. A.; Zorov, S. D.; Balakireva, A. V.; Uhaszova, M. J.; Sollott, S. J.; Zorov, D. B. Mitochondrial membrane potential. *Anal. Biochem.* **2018**, *552*, 50−59.

(22) Li, Q.; Huang, Y. Mitochondrial targeted strategies and theirapplication for cancer and other diseases treatment. *Anal. Biochem.* **2020**, *50*, 271−293.

(23) Safin, D. A.; Mitoraj, M. P.; Robeyns, K.; Filinchuk, Y. C.; Vande Velde, M. Luminescent mononuclear mixed ligand complexes of copper(I) with 5-phenyl-2,2'-bipyridine and triphenylphosphine. *Dalton Trans.* **2015**, *44*, 16824−16832.

(24) Ono, A.; Miyauchi, S.; Demura, M.; Asakura, T.; Kamo, N. Activation Energy for Permeation of Phosphonium Cations through Phospholipid Bilayer Membrane. *Biochemistry* **1994**, *33*, 4312−4318.

(25) Ross, M. F.; Kelso, G. F.; Blaikie, F. H.; James, A. M.; Cochemé, H. M.; Filipovska, A.; Da Ros, T.; Hurd, T. R.; Smith, R. A.; Murphy, M. P. Lipophilic triphenylphosphonium cations as tools in mitochondrial bioenergetics and free radical biology. *Biochemistry* **2005**, *70*, 222−230.

(26) Rottenberg, H. Membrane potential and surface potential in mitochondria: Uptake and binding of lipophilic cations. *J. Membr. Biol.* **1984**, *81* (2), 127−138.

(27) Liberman, E. A.; Topaly, V. P.; Tsofina, L. M.; Iasaïtis, A. A.; Skulachev, V. P. Ion transport and electrical potential of mitochondrial membranes. *Biokhimiia* **1969**, *34*, 1083−1087.
(28) Liberman, E. A.; Topaly, V. P.; Tsofina, L. M.; Jasaitis, A. A.; Skulachev, V. P.,Mechanism of Coupling of Oxidative Phosphorylation and the Membrane Potential of Mitochondria. *Nature* **1969**, *222*, 1076−1078.
(29) Murphy, M. P. Selective targeting of bioactive compounds to mitochondria. *Trends Biotechnol.* **1997**, *15*, 326−330.
(30) Murphy, M. P.; Smith, R. A. Drug delivery to mitochondria: the key to mitochondrial medicine. *Adv. Drug Delivery Rev.* **2000**, *41*, 235−250.
(31) Cheng, X.; Feng, D.; Lv, J.; Cui, X.; Wang, Y.; Wang, Q.; Zhang, L. Application Prospects of Triphenylphosphine-Based Mitochondria-Targeted Cancer Therapy. *Cancers* **2023**, *15*, 666.
(32) Wang, J.; Song, Y.; Huang, Z.; Lin, W.; Yu, G.; Xiong, Y.; Jiang, G.; Tan, Y.; Wang, J.; Liao, X. Coupling a Virulence-Targeting Moiety with Ru-Based AMP Mimics Efficiently Improved Its Anti-Infective Potency and Therapeutic Index. *J. Med. Chem.* **2023**, *66*, 13304−13318.
(33) Marrache, S.; Pathak, R. K.; Dhar, S. Detouring of cisplatin to access mitochondrial genome for overcoming resistance. *Proc. Natl. Acad. Sci. U.S.A.* **2014**, *111*, 10444−10449.
(34) Zhu, Z.; Wang, Z.; Zhang, C.; Wang, Y.; Zhang, H.; Gan, Z.; Guo, Z.; Wang, X. Mitochondrion-targeted platinum complexes suppressing lung cancer through multiple pathways involving energy metabolism. *Chem. Sci.* **2019**, *10*, 3089−3095.
(35) Chen, L. Mitochondrial membrane potential in living cells. *Annu. Rev. Cell Biol.* **1988**, *4*, 155−181.
(36) Gupta, G.; Kumari, P.; Ryu, J. Y.; Lee, J.; Mobin, S. M.; Lee, C. Y. Mitochondrial Localization of Highly Fluorescent and Photostable BODIPY-Based Ruthenium(II), Rhodium(III), and Iridium(III) Metal Complexes. *Inorg. Chem.* **2019**, *58*, 8587−8595.
(37) Maji, M.; Acharya, S.; Bhattacharya, I.; Gupta, A.; Mukherjee, A. Effect of an Imidazole-Containing Schiff Base of an Aromatic Sulfonamide on the Cytotoxic Efficacy of N,N-Coordinated Half-Sandwich Ruthenium(II) p-Cymene Complexes. *Inorg. Chem.* **2021**, *60*, 4744−4754.
(38) Truong, D.; Sullivan, M. P.; Tong, K.; Steel, T. R.; Prause, A.; Lovett, J. H.; Andersen, J. W.; Jamieson, S. M. F.; Harris, H. H.; Ott, I.; Weekley, C. M.; Hummitzsch, K.; Söhnel, T.; Hanif, M.; Metzler-Nolte, N.; Goldstone, D. C.; Hartinger, C. G. Potent Inhibition of Thioredoxin Reductase by the Rh Derivatives of Anticancer M(arene/Cp*)(NHC)Cl_2 Complexes. *Inorg. Chem.* **2020**, *59*, 3281−3289.
(39) Gichumbi, J. M.; Friedrich, H. B. Half-sandwich complexes of platinum group metals (Ir, Rh, Ru and Os) and some recent biological and catalytic applications. *J. Organomet. Chem.* **2018**, *866*, 123−143.
(40) Rademaker-Lakhai, J. M.; van den Bongard, D.; Pluim, D.; Beijnen, J. H.; Schellens, J. H. A Phase I and pharmacological study with imidazolium-trans-DMSO-imidazole-tetrachlororuthenate, a novel ruthenium anticancer agent. *Clin. Cancer Res.* **2004**, *10*, 3717−3727.
(41) Hartinger, C. G.; Jakupec, M. A.; Zorbas-Seifried, S.; Groessl, M.; Egger, A.; Berger, W.; Zorbas, H.; Dyson, P. J.; Keppler, B. K. KP1019, a new redox-active anticancer agent–preclinical development and results of a clinical phase I study in tumor patients. *Chem. Biodivers* **2008**, *5*, 2140−2155.
(42) Peng, K.; Liang, B.; Liu, W.; Mao, Z. What blocks more anticancer platinum complexes from experiment to clinic: Major problems and potential strategies from drug design perspectives. *Coord. Chem. Rev.* **2021**, *449*, 214210.
(43) Ho, G. Y.; Woodward, N. J. I.; Coward. Cisplatin versus carboplatin: comparative review of therapeutic management in solid malignancies. *Crit. Rev. Oncol. Hemat.* **2016**, *102*, 37−46.
(44) Guo, L.; Li, P.; Li, J.; Gong, Y.; Li, X.; Wen, T.; Wu, X.; Yang, X.; Liu, Z. Potent Half-Sandwich $16^-/18^-$Electron Iridium(III) and Ruthenium(II) Anticancer Complexes with Readily Available Amine−Imine Ligands. *Inorg. Chem.* **2023**, *62*, 21379−21395.
(45) Guo, L.; Li, P.; Li, J.; Gong, Y.; Lai, K.; Fu, H.; Dong, H.; Yang, Z.; Liu, Z. Iminoamido chelated iridium(III) and ruthenium(II) anticancer complexes with mitochondria-targeting ability and potential to overcome cisplatin resistance. *J. Inorg. Biochem.* **2024**, *258*, 112631.
(46) Hu, X.; Guo, L.; Liu, M.; Sun, M.; Zhang, Q.; Peng, H.; Zhang, F.; Liu, Z. Formation of Iridium(III) and Rhodium(III) Amine, Imine, and Amido Complexes Based on Pyridine−Amine Ligands: Structural Diversity Arising from Reaction Conditions, Substituent Variation, and Metal Centers. *Inorg. Chem.* **2022**, *61*, 10051−10065.
(47) Li, P.; Guo, L.; Li, J.; Yang, Z.; Fu, H.; Lai, K.; Dong, H.; Fan, C.; Liu, Z. Mitochondria-targeted neutral and cationic iridium(III) anticancer complexes chelating simple hybrid sp^2-N/sp^3-N donor ligands. *Dalton Trans.* **2024**, *53*, 1977−1988.
(48) Guo, L.; Li, P.; Li, J.; Gong, Y.; Li, X.; Liu, Y.; Yu, K.; Liu, Z. Half-Sandwich Iridium(III), Rhodium(III), and Ruthenium(II) Complexes Chelating Hybrid sp^2-N/sp^3-N Donor Ligands to Achieve Improved Anticancer Selectivity. *Inorg. Chem.* **2023**, *62*, 15118−15137.
(49) Tian, M.; Li, J.; Zhang, S.; Guo, L.; He, X.; Kong, D.; Zhang, H.; Liu, Z. Half-sandwich ruthenium(II) complexes containing N^N-chelated imino-pyridyl ligands that are selectively toxic to cancer cells. *Chem. Commun.* **2017**, *53*, 12810−12813.
(50) Tian, Z.; Li, J.; Zhang, S.; Xu, Z.; Yang, Y.; Kong, D.; Zhang, H.; Ge, X.; Zhang, J.; Liu, Z. Lysosome-Targeted Chemotherapeutics: Half-Sandwich Ruthenium(II) Complexes That Are Selectively Toxic to Cancer Cells. *Inorg. Chem.* **2018**, *57*, 10498−10502.
(51) Gao, J.; Guo, L.; Wu, Y.; Cheng, Y.; Hu, X.; Liu, J.; Liu, Z. 16-Electron Half-Sandwich Rhodium(III), Iridium(III), and Ruthenium-(II) Complexes as Lysosome-Targeted Anticancer Agents. *Organometallics* **2021**, *40*, 3999−4010.
(52) Hu, X.; Guo, L.; Liu, M.; Zhang, Q.; Gong, Y.; Sun, M.; Feng, S.; Xu, Y.; Liu, Y.; Liu, Z. Increasing Anticancer Activity with Phosphine Ligation in Zwitterionic Half-Sandwich Iridium(III), Rhodium(III), and Ruthenium(II) Complexes. *Inorg. Chem.* **2022**, *61*, 20008−20025.
(53) Du, Q.; Guo, L.; Ge, X.; Zhao, L.; Tian, Z.; Liu, X.; Zhang, F.; Liu, Z. Serendipitous Synthesis of Five-Coordinated Half-Sandwich Aminoimine Iridium(III) and Ruthenium(II) Complexes and Their Application as Potent Anticancer Agents. *Inorg. Chem.* **2019**, *58*, 5956−5965.
(54) Lenis-Rojas, O. A.; Robalo, M. P.; Tomaz, A. I.; Carvalho, A.; Fernandes, A. R.; Marques, F.; Folgueira, M.; Yáñez, J.; Vázquez-García, D.; López Torres, M.; Fernández, A.; Fernández, J. J. RuII(p-cymene) Compounds as Effective and Selective Anticancer Candidates with No Toxicity in Vivo. *Inorg. Chem.* **2018**, *57*, 13150−13166.
(55) Selvam, P.; De, S.; Paira, P. S.; Kumar, K. A.; Kumar, R. S.; Moorthy, A.; Ghosh, A.; Kuo, Y. C.; Banerjee, S. S.; Jenifer, K. In vitro studies on the selective cytotoxic effect of luminescent Ru(II)-p-cymene complexes of imidazo-pyridine and imidazo quinoline ligands. *Dalton Trans.* **2022**, *51*, 17263−17276.
(56) Panchangam, R. L.; Rao, R. N.; Balamurali, M. M.; Hingamire, T. B.; Shanmugam, D.; Manickam, V.; Chanda, K. Antitumor Effects of Ir(III)-2H-Indazole Complexes for Triple Negative Breast Cancer. *Inorg. Chem.* **2021**, *60*, 17593−17607.
(57) Gao, J.; Guo, L.; Wu, Y.; Cheng, Y.; Hu, X.; Liu, J.; Liu, Z. 16-electron half-sandwich rhodium(III), iridium(III), and ruthenium(II) complexes as lysosome-targeted anticancer agents. *Organometallics* **2021**, *40*, 3999.
(58) Arunachalam, A.; Rengan, R.; Umapathy, D.; Arockiam, A. J. V. Impact of biphenyl benzhydrazone-incorporated arene Ru(II) complexes on cytotoxicity and the cancer cell death mechanism. *Organometallics* **2022**, *41*, 2474.
(59) Guo, L.; Zhang, H.; Tian, M.; Tian, Z.; Xu, Y.; Yang, Y.; Peng, H.; Liu, P.; Liu, Z. Electronic effects on reactivity and anticancer activity by half-sandwich N,N-chelated iridium(III) complexes. *New J. Chem.* **2018**, *42*, 16183−16192.

https://doi.org/10.1021/acs.inorgchem.4c03975
Inorg. Chem. 2024, 63, 24736−24753

(60) Zhao, C.-X.; Liu, J.-N.; Li, B.; Ren, D.; Chen, X.; Yu, J.; Zhang, Q. Multiscale Construction of Bifunctional Electrocatalysts for Long-Lifespan Rechargeable Zinc−Air Batteries. *Adv. Funct. Mater.* **2020**, *30*, 2003619.
(61) Guo, L.; Zhang, H.; Tian, M.; Tian, Z.; Xu, Y.; Yang, Y.; Peng, H.; Liu, P.; Liu, Z. Electronic effects on reactivity and anticancer activity by half-sandwich N,N-chelated iridium(III) complexes. *New J. Chem.* **2018**, *42*, 16183.
(62) Li, J.; Guo, L.; Tian, Z.; Tian, M.; Zhang, S.; Xu, K.; Qian, Y.; Liu, Z. Novel half-sandwich iridium(III) imino-pyridyl complexes showing remarkable in vitro anticancer activity. *Dalton Trans.* **2017**, *46*, 15520−15534.
(63) Petrović, A.; Milutinović, M. M.; Petri, E. T.; Živanović, M.; Milivojević, N.; Puchta, R.; Scheurer, A.; Korzekwa, J.; Klisurić, O. R.; Bogojeski, J. Synthesis of Camphor-Derived Bis(pyrazolylpyridine) Rhodium(III) Complexes: Structure-Reactivity Relationships and Biological Activity. *Inorg. Chem.* **2019**, *58*, 307−319.
(64) Mukhopadhyay, S.; Gupta, R. K.; Paitandi, R. P.; Rana, N. K.; Sharma, G.; Koch, B.; Rana, L. K.; Hundal, M. S.; Pandey, D. S. Synthesis, Structure, DNA/Protein Binding, and Anticancer Activity of Some Half-Sandwich Cyclometalated Rh(III) and Ir(III) Complexes. *Organometallics* **2015**, *34*, 4491−4506.
(65) Thota, S.; Rodrigues, D. A.; Crans, D. C.; Barreiro, E. J. (II) Compounds: Next-Generation Anticancer Metallotherapeutics? *J. Med. Chem.* **2018**, *61*, 5805−5821.
(66) Selvam, P.; De, S.; Paira, P.; Kumar, S. K. A.; Kumar, R. S.; Moorthy, A.; Ghosh, A.; Kuo, Y. C.; Banerjee, S.; Jenifer, S. K. In vitro studies on the selective cytotoxic effect of luminescent Ru(II)-p-cymene complexes of imidazo-pyridine and imidazo quinoline ligands. *Dalton Trans.* **2022**, *51*, 17263−17276.
(67) Senthil Raja, D.; Bhuvanesh, N. S. P.; Natarajan, K. Biological evaluation of a novel water soluble sulphur bridged binuclear copper(II) thiosemicarbazone complex. *Eur. J. Med. Chem.* **2011**, *46*, 4584−4594.
(68) Timerbaev, A. R.; Hartinger, C. G.; Aleksenko, S. S.; Keppler, B. K. Interactions of Antitumor Metallodrugs with Serum Proteins: Advances in Characterization Using Modern Analytical Methodology. *Chem. Rev.* **2006**, *106*, 2224−2248.
(69) Yang, Y.; Guo, L.; Tian, Z.; Gong, Y.; Zheng, H.; Zhang, S.; Xu, Z.; Ge, X.; Liu, Z. Novel and Versatile Imine-N-Heterocyclic Carbene Half-Sandwich Iridium(III) Complexes as Lysosome-Targeted Anticancer Agents. *Inorg. Chem.* **2018**, *57*, 11087−11098.
(70) Samari, F.; Hemmateenejad, B.; Shamsipur, M.; Rashidi, M.; Samouei, H. Affinity of Two Novel Five-Coordinated Anticancer Pt(II) Complexes to Human and Bovine Serum Albumins: A Spectroscopic Approach. *Inorg. Chem.* **2012**, *51*, 3454−3464.
(71) Castiñeiras, A.; Fernández-Hermida, N.; García-Santos, I.; Gómez-Rodríguez, L. Neutral Ni(II), Pd(II) and Pt(II) ONS-pincer complexes of 5-acetylbarbituric-4N-dimethylthiosemicarbazone: synthesis, characterization and properties. *Dalton Trans.* **2012**, *41*, 13486−13495.
(72) Cheng, Z. Studies on the interaction between scopoletin and two serum albumins by spectroscopic methods. *J. Lumin* **2012**, *132*, 2719−2729.
(73) Hayes, J. D.; Dinkova-Kostova, A. T.; Tew, K. D. Oxidative Stress in Cancer. *Cancer Cell* **2020**, *38*, 167−197.
(74) Swaminathan, S.; Deepak, R. J.; Karvembu, R. Interweaving catalysis and cancer using Ru- and Os-arene complexes to alter cellular redox state: A structure-activity relationship (SAR) review. *Coord. Chem. Rev.* **2023**, *491*, 215230.
(75) Fu, Y.; Romero, M. J.; Habtemariam, A.; Snowden; Song, L.; Clarkson, G. J.; Qamar, B.; Pizarro, A. M.; Unwin, P. R.; Sadler, P. J. The contrasting chemical reactivity of potent isoelectronic iminopyridine and azopyridine osmium(II) arene anticancer complexes. *Chem. Sci.* **2012**, *3*, 2485−2494.
(76) Liu, Z.; Romero-Canelón, I.; Qamar, B.; Hearn, J. M.; Habtemariam, A.; Barry, N. P.; Pizarro, A. M.; Clarkson, G. J.; Sadler, P. J. The Potent Oxidant Anticancer Activity of Organoiridium Catalyst. *Angew. Chem., Int. Ed.* **2014**, *53*, 3941−3946.
(77) Liu, Z.; Romero-Canelón, I.; Qamar, B.; Hearn, J. M.; Habtemariam, A.; Barry, N. P. E.; Pizarro, A. M.; Clarkson, G. J.; Sadler, P. J. The Potent Oxidant Anticancer Activity of Organoiridium Catalysts. *Angewandte Chem. Int. Ed.* **2014**, *53*, 3941−3946.
(78) Liu, Z.; Sadler, P. J. Organoiridium Complexes: Anticancer Agents and Catalysts. *Acc. Chem. Res.* **2014**, *47*, 1174−1185.
(79) Lo, K. K. W.; Zhang, K. Y. Iridium(III) complexes as therapeutic and bioimaging reagents for cellular applications. *RSC Adv.* **2012**, *2*, 12069−12083.
(80) Murphy, M. P. Slip and leak in mitochondrial oxidative phosphorylation. *BBA- Bioenergetics* **1989**, *977*, 123−141.
(81) Qiu, K.; Chen, Y.; Rees, T. W.; Ji, L.; Chao, H. Organelle-targeting metal complexes: From molecular design to bio-applications. *Coord. Chem. Rev.* **2019**, *378*, 66−86.
(82) Li, G.; Lin, Q.; Sun, L.; Feng, C.; Zhang, P.; Yu, B.; Chen, Y.; Wen, Y.; Wang, H.; Ji, L.; Chao, H. A mitochondrial targeted two-photon iridium(III) phosphorescent probe for selective detection of hypochlorite in live cells and in vivo. *Biomaterials* **2015**, *53*, 285−295.
(83) Wang, L.; Wang, X.; Chen, F.; Song, Y. Q.; Nao, S. C.; Chan, D. S.; Wong, C. Y.; Wang, W.; Leung, C.-H. A glycyrrhetinic acid-iridium(III) conjugate as a theranostic NIR probe for hepatocellular carcinoma with mitochondrial-targeting ability. *Eur. J. Med. Chem.* **2024**, *264*, 115995.
(84) Kuang, K.; Li, C.; Maksut, F.; Ghosh, D.; Vinck, R.; Wang, M.; Poupon, J.; Xiang, R.; Li, W.; Li, F.; Wang, Z.; et al. A G-quadruplex-binding platinum complex induces cancer mitochondrial dysfunction through dual-targeting mitochondrial and nuclear G4 enriched genome. *J. Biomed. Sci.* **2024**, *31* (1), 50.
(85) Tian, J.; Li, M.; Tian, Z.; Zhang, S.; Yan, C.; Shao, C.; Liu, Z. Half-Sandwich Iridium(III) and Ruthenium(II) Complexes Containing P^P-Chelating Ligands: A New Class of Potent Anticancer Agents with Unusual Redox Features. *Inorg. Chem.* **2018**, *57*, 1705−1716.
(86) Hetz, C.; Vitte, P. A.; Bombrun, A.; Rostovtseva, T. K.; Montessuit, S.; Hiver, A.; Schwarz, M. K.; Church, D. J.; Korsmeyer, S. J.; Martinou, J. C.; Antonsson, B. Bax Channel Inhibitors Prevent Mitochondrion-mediated Apoptosis and Protect Neurons in a Model of Global Brain Ischemia*. *J. Biol. Chem.* **2005**, *280*, 42960−42970.
(87) Li, C. Y.; Yu, M. X.; Sun, Y.; Wu, Y. Q.; Huang, C. H.; Li, F. Y. A nonemissive iridium(III) complex that specifically lights-up the nuclei of living cells. *J. Am. Chem. Soc.* **2011**, *133*, 11231−11239.
(88) Puckett, C. A.; Barton, J. K. Mechanism of cellular uptake of a ruthenium poly-pyridyl complex. *Biochemistry* **2008**, *47*, 11711−11716.
(89) Dan Dunn, J.; Alvarez, L. A.; Zhang, X.; Soldati, T. Reactive oxygen species and mitochondria: A nexus of cellular homeostasis. *Redox Biol.* **2015**, *6*, 472−485.
(90) Scheffler, I. E. A century of mitochondrial research: achievements and perspectives. *Mitochondrion* **2001**, *1*, 3−31.
(91) Romero-Canelon, I.; Mos, M.; Sadler, P. J. Enhancement of Selectivity of an Organometallic Anticancer Agent by Redox Modulation. *J. Med. Chem.* **2015**, *58*, 7874−7880.
(92) Romero-Canelon, I.; Sadler, P. J. Next-generation metal anticancer complexes: multitargeting via redox modulation. *Inorg. Chem.* **2013**, *52*, 12276−12291.
(93) Acharya, A.; Das, I.; Chandhok, D.; Saha, T. Redox regulation in cancer: a double-edged sword with therapeutic potential. *Oxid. Med. Cell. Longev.* **2010**, *3*, 23−34.
(94) Ye, Y.; Zhang, T.; Yuan, H.; Li, D.; Lou, H.; Fan, P. Mitochondria-Targeted Lupane Triterpenoid Derivatives and Their Selective Apoptosis-Inducing Anticancer Mechanisms. *J. Med. Chem.* **2017**, *60*, 6353−6363.
(95) Belloc, F.; Belaud-Rotureau, M. A.; Lavignolle, V.; Bascans, E.; Braz-Pereira, E.; Durrieu, F.; Lacombe, F. Flow cytometry detection of caspase 3 activation in preapoptotic leukemic cells. *Cytometry* **2000**, *40*, 151−160.
(96) Kozieł, S.; Komarnicka, U. K.; Ziółkowska, A.; Skórska-Stania, A.; Pucelik, B.; Płotek, M.; Sebastian, V.; Bieńko, A.; Stochel, G.; Kyzioł, A. Anticancer potency of novel organometallic Ir(III)

https://doi.org/10.1021/acs.inorgchem.4c03975
Inorg. Chem. 2024, 63, 24736−24753

complexes with phosphine derivatives of fluoroquinolones encapsulated in polymeric micelles. *Inorg. Chem. Front.* **2020**, *7*, 3386−3401.
(97) Valastyan, S.; Weinberg, R. Robert A Weinberg, Tumor Metastasis: Molecular Insights and Evolving Paradigms. *Cell* **2011**, *147*, 275−292.
(98) Patil, S.; Pandey, S.; Singh, A.; Radhakrishna, M.; Basu, S. Hydrazide−Hydrazone Small Molecules as AIEgens: Illuminating Mitochondria in Cancer Cells. *Chem.—Eur. J.* **2019**, *25*, 8229−8235.

https://doi.org/10.1021/acs.inorgchem.4c03975
Inorg. Chem. 2024, 63, 24736−24753